RESEARCH ARTICLE

Internal phosphorus loading alters nutrient limitation and contributes to cyanobacterial blooms in a polymictic lake

Micah M. Swann[1,2] · Alicia Cortes[1,2] · Alexander L. Forrest[1,2] · Nick Framsted[1,3] · Steven Sadro[2,3] · S. Geoffrey Schladow[1,2] · Angela De Palma-Dow[4]

Abstract

Clear Lake, a medium-sized hypereutrophic, polymictic lake in northern California, has had recurring harmful cyanobacteria blooms (HCBs) for over a century despite reductions in external phosphorus (P) loadings. Internal P loading can alter nutrient availability and limitation supporting HCBs but is rarely quantified or compared with external loads. We have quantified external P loads from 2019 to 2021 for the three main tributaries (accounting for 46% of the flow) and internal loadings using two methods: a P mass balance and modeled release rates of soluble reactive phosphorus from oxic and anoxic sediments. In addition, we combined high-frequency in situ measurements of water temperature and dissolved oxygen, discrete grab sampling for nutrient chemistry, and remote sensing to explore the potential drivers of the observed variability and provide a comprehensive view of the spatiotemporal dynamics of HCBs. By understanding the relative contribution of external and internal nutrient loadings and the relationship between environmental parameters and HCBs, interannual bloom variability can be better predicted. Comparative estimates of external and internal phosphorus loading indicate that internal sources accounted for 70–95% of the total P input into the system during the study period. Contrary to other lakes, the intensity of the summer bloom season was correlated to the timing and duration of anoxia rather than the magnitude of spring runoff. Internally released P shifted the system from phosphorus to nitrogen limitation during the summer, potentially favoring the proliferation of nitrogen-fixing cyanobacteria.

Keywords Hypereutrophic · Polymictic · Cyanobacteria · Internal phosphorus loading · Clear lake

Introduction

Eutrophication poses a grave threat to lentic ecosystems globally, promoting the proliferation of harmful cyanobacteria blooms (HCBs) that reduce aquatic biodiversity, yielding increased water treatment costs, and threatening human health through bloom-produced cyanotoxins (Aráoz et al. 2010; Chorus et al. 2000; Paerl et al. 2001; Svirčev et al.

2014). Phosphorus (P) has been historically viewed as the limiting nutrient for primary production in freshwater lakes (Dillon and Rigler 1974; Smith 1985; Smith and Schindler 2009), and watershed P load reduction programs have been widely implemented to control HCBs (Schindler et al. 2016; Xu et al. 2015). While external nutrient loading (L_{ext}) ultimately regulates lake water quality over longer timescales, internal loading (L_{int}) from sediment nutrient pools defines the timeframe required for load abatement programs to result in improved water quality and can directly influence the intensity of the summer HCB season (Coveney et al. 2005; Isles et al. 2015; Søndergaard et al. 2003). Despite the potential for internal P loading to delay the recovery of eutrophic lakes, L_{int} is rarely quantified and directly compared to L_{ext}, especially over timescales that adequately resolve the physicochemical and biological mechanisms which contribute to in-lake P cycling.

When P enters a lake, it can be cycled within food webs or retained in sediment. Under oxidizing conditions, P is

✉ Micah M. Swann
mswann@ucdavis.edu

1 Davis Department of Civil and Environmental Engineering, University of California, Davis, CA, USA

2 Davis Tahoe Environmental Research Center, University of California, Incline Village, NV, USA

3 Davis Department of Environmental Science and Policy, University of California, Davis, CA, USA

4 County of Lake Water Resources Department, Lakeport, CA, USA

adsorbed onto ferric oxy-hydroxides and deposited in sediments (Einsele 1936; Mortimer 1941). In summer, when thermal stratification prevents the vertical exchange of dissolved oxygen (DO), anoxic sediments release chemically bound P into porewater, which is eventually internally loaded into the overlying water column via advection and diffusion. Aerobic organic matter decomposition can also promote the release of inorganic and dissolved organic P into the water column (Hupfer and Lewandowski 2008; Song and Burgin 2017). While watershed L_{ext} can be directly quantified via stream discharge and nutrient concentration data, L_{int} is more difficult to assess because internal P sources cannot be easily measured in situ before biotic uptake (Nürnberg 2009a, b). Methods for quantifying L_{int} include regression analysis, mass-balance techniques, time-dynamic modeling, and coupled hydrodynamic-ecological modeling (Burger et al. 2008; Håkanson 2004; Nürnberg 1988, 2009a, b).

In polymictic systems, L_{int} is frequently ignored or assumed negligible in mass balance studies since hypolimnetic DO concentrations in temporarily stratifying systems rarely remain consistently anoxic (DO < 1 mg L^{-1}) during the warm growing season (Molot et al. 2010; Nürnberg 2005; Orihel et al. 2015; Winter et al. 2002). However, elevated total phosphorus (TP) concentrations have been observed in eutrophic, polymictic systems when bottom water DO is depleted (Burger et al. 2008; Nürnberg et al. 2013a, b). Resolving the spatial and temporal extent of anoxia and hypoxia (DO < 3.5 mg L^{-1}) in frequently mixing systems remains challenging, as hypolimnetic DO can rapidly decline during stratification, and reoxygenation regularly occurs with mixing events (Nürnberg and LaZerte 2016; Tammeorg et al. 2020).

Episodic summertime mixing events can make polymictic systems highly susceptible to HCBs when nutrient-enriched waters are transported vertically into the epilimnion during the warm growing season. In addition to increasing bioavailable nutrients, a surplus of P relative to nitrogen (N) in surface waters shifts the system towards nitrogen limitation, which favors the dominance of nitrogen-fixing cyanobacteria that often produce cyanotoxins (Orihel et al. 2015; Smith 1983). Non-N-fixing cyanobacteria, such as *Microcystis*, can subsequently dominate due to their ability to maintain net growth under low underwater irradiance (van Duin et al. 1995). An N:P molar ratio < 16:1 is commonly proposed to indicate N limitation in marine environments (Redfield 1958). However, this may be a poor approximation for nutrient limitation in freshwater systems as nutrient demands differ for inland and marine ecosystems (Domagalski et al. 2021). Guildford and Hecky (2000) suggested that in lakes, N limitation occurs at TN:TP molar ratios < 20:1, though the molar TN:TP threshold indicating shifts in nutrient limitation is likely system-specific (Klausmier et al. 2004).

This study explores the linkages between internal P loading and the interannual variability of HCB severity in a hypereutrophic, polymictic system. We combined data from a range of sources collected over a 3-year period to quantify the internal and external nutrient loads and their relationship to the magnitude of the summer HCB season in Clear Lake, California. We estimated (1) net annual internal P loads from observed changes in the integrated lake P during the dry season, and (2) gross P loads derived from experimental sediment soluble reactive phosphorus (SRP) release rates and estimates of hypolimnetic hypoxia. The terms net and gross respectively differentiate whether or not the P fraction removed from the water column via sedimentation is considered in the associated calculations. For the latter method, we applied a novel approach, comparing theoretical estimates of sediment anoxia [i.e., Nürnberg's anoxic factor (Nürnberg 2005)] with in situ hypolimnetic DO measurements to calibrate the system-specific threshold for which redox-mediated internal P loading will occur. In addition, we examined how interbasin and interannual variability in the timing and duration of mixing events influences the summer HCB season.

We hypothesize that (1) P release from anoxic sediments is the primary source of phosphorus loading to Clear Lake; (2) internal P loading is one of the main drivers of blooms of nitrogen-fixing cyanobacteria by lowering N:P ratios, creating a nitrogen-limited environment; and (3) the annual variation in the timing and duration of hypoxia regulates the magnitude of the summer HCB season. We then compare the strengths and limitations of each internal loading estimate to provide insight for improving loading estimation methods in polymictic systems. Finally, the contribution of internal loading to Clear Lake's overall phosphorus budget is assessed to determine if current lake management policies can be expected to improve water quality in the long term.

Materials and methods

Study site

Clear Lake is a shallow, polymictic lake located in the coastal range of northern California (39°00′N; 122°45′W). The lake has an average surface area (A_o) of 151 km^2, mean depth (Z_{mean}) of 8 m, and maximum depth (Z_{max}) of 15 m (Table 1). Annual precipitation variability and water releases result in year-to-year water surface elevation fluctuations from nearly 1 m below the natural rim of the lake to nearly 3 m above it. As a result of the lake's relatively shallow depth, long fetch, and the prevailing west/northwesterly winds, Clear Lake mixes to the bottom frequently during the summer months when the water column is thermally stratified. The lake has three distinct sub-basins: Upper, Oaks, and Lower Arm (Fig. 1). The Upper Arm (UA) is the largest and shallowest basin and receives over 90% of

Table 1 Physical characteristics of Clear Lake and sub-basins. Values in parentheses indicate percentage of total lake

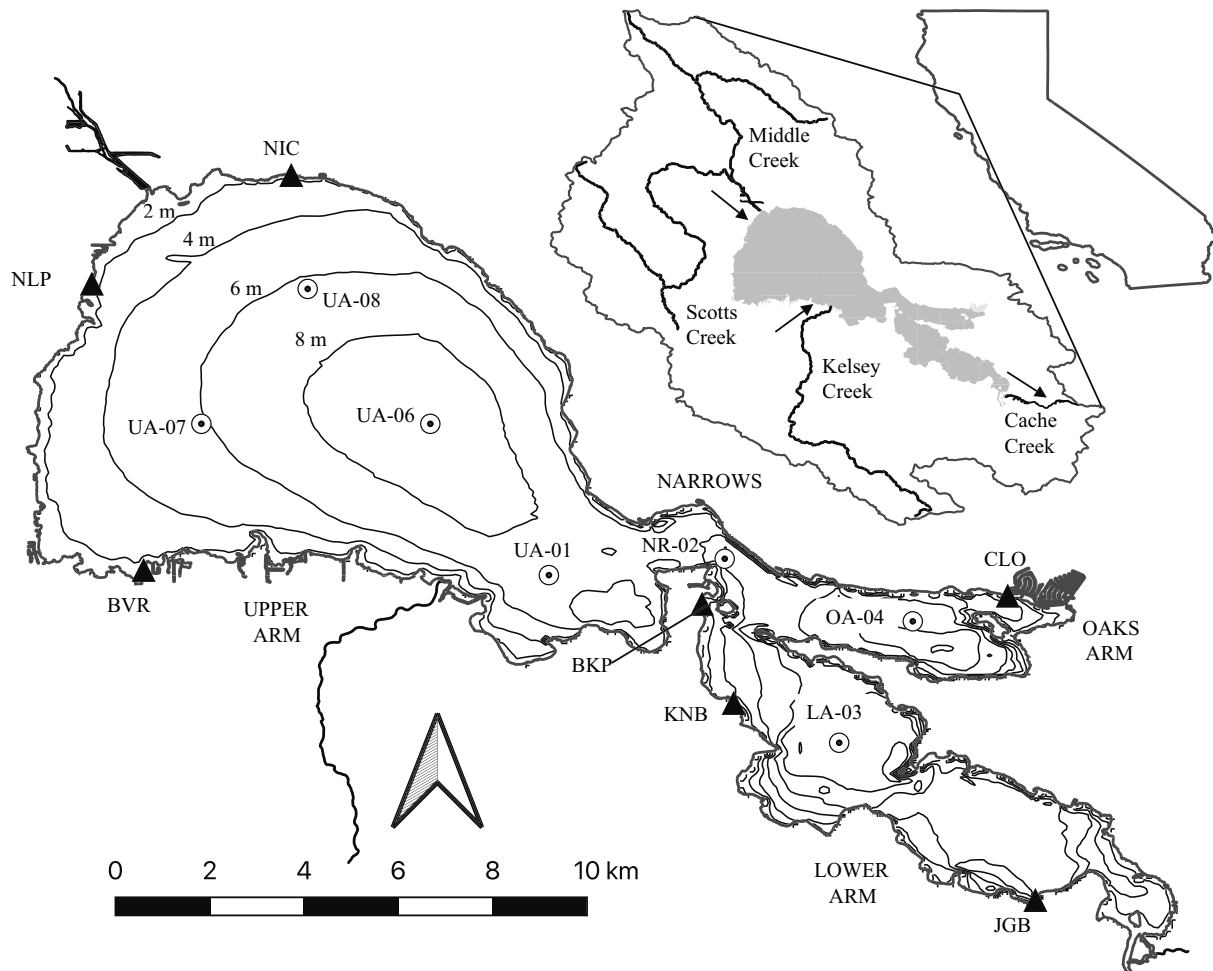| Characteristic	Upper Arm (UA)	Oaks Arm (OA)	Lower Arm (LA)	Whole lake
Station(s)	UA-01, UA-06, UA-08	OA-04	LA-03	All
Catchment area (A_o, km^2)	1031	89	83	1190
Surface Area (A_o, km^2)	106 (70%)	15 (10%)	30 (20%)	151 (100%)
Max depth (Z_{mean}, m)	11	14	15	15
Mean depth (Z_{max}, m)	6	9	8.5	8
Volume (V, km^3)	0.66 (63%)	0.13 (12%)	0.27 (25%)	1.11 (100%)
Dynamic ratio (DR, km/m)	1.7	0.4	0.7	1.5

Fig. 1 Subsurface instrument mooring, water column and sediment core sampling sites in Clear Lake, California with 2 m bathymetry contour lines. The two-character site prefix indicates locations in Upper Arm (UA), Oaks Arm (OA), Lower Arm (LA), and Narrows (NR). Locations of subsurface monitoring moorings are marked with white circles, and locations of shoreline meteorological stations are shown by black triangles. The insert to the right of the bathymetrical map shows the location of the Clear Lake watershed in California, its extent, and the location of the main creeks

the watershed runoff. This includes flows from the lake's three largest inlets: Middle, Scotts, and Kelsey Creek. A passage at the east end of the UA (the Narrows), connects to the two smaller and deeper basins. The Lower Arm (LA) discharges into the lake's only outflow, Cache Creek, while the Oaks Arm (OA) is the smallest basin and extends east of the Narrows. The residence time of the whole lake has been estimated at 4.5 years (Chamberlin et al. 1990).

The lake is naturally highly productive due to its large drainage basin area, which contributes to a significant

external load of mineral nutrients from nutrient-rich volcanic soils within the watershed (Wilson 2015). Paleolimnological evidence indicates that the lake has supported abundant phytoplankton production for the past 15,000 years (Sims 1988). However, since the mid-1800s, anthropogenic modifications to the watershed (e.g., wetland conversion, shoreline development, agriculture, and mining) have significantly increased sediment and nutrient loading to the lake, exacerbating eutrophication and promoting the proliferation of HCBs (Suchanek et al. 2002). The earliest lake nutrient measurements, collected from 1969 to 1972, recorded peak summer dissolved P concentrations up to 0.5 mg L^{-1}. Clear Lake has also warmed during this period; average summer surface temperatures increased by 1.39 °C (95% CI ± 0.63) from 1970 to 2020 (Online Resource Fig, S.1), favoring cyanobacteria proliferation (Smucker et al. 2021). Monitoring of shoreline cyanobacteria and cyanotoxins is presently conducted by the Big Valley and Elem Indian Colony Environmental Protection Departments (https://bit.ly/ClearLakeCyanoProgram), which provides biweekly toxin risk assessment maps.

Cyanobacteria assemblages typically form between April and October and have been historically dominated by N-fixing cyanobacteria *Dolichospermum*, *Lyngbya*, and *Gloeotrichia*, as well as the non-N-fixing cyanobacteria *Microcystis*, *Planktothrix*, and *Pseudanabaena* (Richerson et al. 1994; Winder et al. 2010). All these genera are capable of producing cyanotoxins (Bláha et al. 2009). Horne and Goldman (1972) determined that atmospheric fixation accounts for 40% of Clear Lake's annual nitrogen inputs. Blooms tend to first form and be most persistent in the eastern arms of the lake (OA and LA), where surface scums accumulate due to prevailing winds but can also frequently occur in natural coves within the UA (Richerson et al. 1994; Tetra Tech 2004). The bloom season is generally defined by two peaks in biomass occurring in late spring and early fall, separated by a minimum in August (Horne 1975). Wurtsbaugh and Horne (1983) hypothesized that the exhaustion of available iron during the midsummer limited atmospheric nitrogen uptake and catalyzed the die-off of N-fixing species in the late summer.

To reduce the nutrient loads in Clear Lake, a total maximum daily load (TMDL) was established in 2006, limiting watershed inputs to a target TP load of 239.1 kg day^{-1} (548 mg m^{-2} year^{-1} Tetra Tech 2004). In addition, a pipeline was completed in 2003 to divert wastewater discharges from the lake to nearby geothermal steam fields (Water Resources Department of Lake County 2010). While watershed restoration efforts (e.g., erosion control and wetland restoration) have been implemented to reduce external P sources and attain TMDL targets, HCBs continue to regularly occur each summer, and annual maximum lake TP concentrations have not declined in 17 years following the implementation of the regulation.

Field data collection

Six bottom-moored thermistor and oxygen sensor arrays were deployed in the three basins of the lake in March 2019, continuously measuring water temperature and dissolved oxygen (DO) through the water column (Fig. 1). The moorings are comprised of RBR solo³T thermistors (0.002 °C accuracy, 0.0002 °C resolution) spaced ~ 1 m apart with RBR codaT.ODO dissolved oxygen sensors (accuracy 0.26 mg L^{-1} and resolution < 0.03 mg L^{-1}) at a height (z) of 0.5 m above the lakebed. The deepest site in each arm (OA-04, LA-03, and UA-06) also contained RBR-DO loggers at $z = 2$ m and PME miniDOT dissolved oxygen sensors (accuracy 0.3 mg L^{-1} and resolution of 0.01 mg L^{-1}) at ~ 4–5 m below the surface. Thermistors and RBR DO and PME DO loggers sampled at intervals of 10 s, 30 s, and 1 min, respectively. A detailed description of the mooring setup can be found in Online Resource Sect. 2. Water samples were collected using a peristaltic pump and silicon tubing lowered to four depths (0.5 m below the surface and $z = 1$, 2, and 4 m above the bottom) every ~ 8 weeks in winter and ~ 6 weeks in summer. Once collected, samples were stored in the dark on ice and transported to the laboratory for processing. Dissolved samples were filtered through a 0.45 μm filter within 24 h of sampling to limit reabsorption of dissolved material. Samples were analyzed for a range of dissolved and particulate carbon, N and P forms, and chlorophyll using the analytical methods outlined in Online Resource Sect. 3.

Meteorological data were obtained from seven stations deployed along the perimeter of the lake at Nice (NIC), North Lakeport (NLP), Big Valley Rancheria, (BVR), Konocti Bay (KNB), Jago Bay (JGB), Buckingham Point (BKP), and Clearlake Oaks (CLO). Air temperature, relative humidity, incoming shortwave solar radiation, and wind speed and direction were measured every 15 min with Davis Instruments Wireless Vantage Pro2 Plus® meteorological stations. At each site (except BVR), a surface water temperature sensor (Onset Water Temp Pros® with 0.2 °C accuracy, 0.02 °C resolution) was deployed ~ 0.5 m below the lake surface, sampling every 10 min. Hourly precipitation data were obtained from the Mt. Konocti Meteorological Station operated by the Western Regional Climate Center.

Cyanobacteria dynamics

To quantify large-scale variability of HCBs in Clear Lake, we utilized remote sensing data collected by the Ocean Land Color Instrument on board the Copernicus Sentinel-3 satellite and post-processed by the National Oceanic and Atmospheric Association (San Francisco Estuary Institute 2022). Satellite imagery estimates the abundance of cyanobacteria (i.e., Modified Cyanobacteria Index [*CI*]) by measuring the absorption of light by chlorophyll and phycocyanin, a photosynthetic

pigment specific to cyanobacteria (Stumpf et al. 2009). Abundance data can be estimated for the top 1 m of the water column with a pixel resolution of 300 m. We assessed 10-day running maximum composites of daily products to avoid data contaminated by clouds and glint. All pixels adjacent to the lake shoreline were excluded from this analysis, as edge water pixels may be contaminated with spectra of adjoining land features (Iiames et al. 2021). While this remote sensing product has not formally been validated for Clear Lake's lake-specific cyanobacteria community, Lunetta et al. (2015) demonstrated that this algorithm provided robust estimates for cyanobacteria cell counts in lakes spanning eight states in the Eastern United States. We determined that this tool provided accurate quantitative information on the seasonal dynamics of cyanobacteria blooms in Clear Lake by comparing measured cyanobacteria biovolumes from surface samples with the modified CI from overlapping pixels collected on the same day (Online Resource Sect. 4). While the tool did not detect cyanobacteria below concentrations of 10^8 μm^3 L^{-1}, the modified CI was significantly correlated with biovolume above this threshold ($R^2 = 0.51$, $p < 0.01$, $n = 50$). We expect this correlation to improve once the remote sensing product is fully validated for Clear Lake's cyanobacteria community, as was initially conducted in Sharp et al. (2021). These data were assessed by calculating the spatially averaged CI and percent coverage of blooms in each arm. To quantify the lake-wide and arm-specific severity of each summer HCB season, we calculated the bloom magnitude metric (BM, Mishra et al. 2019) by calculating the spatiotemporal mean CI from June to October each year as

$$BM = \frac{1}{T} \sum_{t=1}^{T} \sum_{p=1}^{P} CI \tag{1}$$

where the indices P and T respectively represent the number of valid pixels with detectable CI in a basin and the number of composite time sequences in each month.

External load estimates

Annual external P loads (Jan–Dec) were quantified for the three primary tributaries (Kelsey, Middle, and Scotts Creek) using 15-min stream gauging data collected by the California Department of Water Resources (DWR) and stream-specific linear regressions relating discharge to TP derived from routine stream monitoring data collected by the Lake County Water Resources Department (LCWRD) from 2008 to 2018 (Online Resource Sect. 5). While these streams account for 73% of the total inflow into Clear Lake (Richerson et al. 1994), gauges are located several miles upstream of the lake inlet, and therefore the gauged area accounts for 46% of the Clear Lakes inflows (Lake County Watershed Protection District 2009; Tetra Tech 2004). The cumulative nutrient load

was multiplied by a factor of 2.18 to account for the ungauged portion of the watershed. P inputs from atmospheric deposition (L_{atm}) were calculated using wet (0.25 mg TP m^{-2} day^{-1}) and dry (2 mg TP m^{-2} day^{-1}) P deposition rates from Lake Tahoe (Jassby et al. 1994), located approximately 220 km east of Clear Lake. These rates are higher than the average of 38 North American sites (0.12 ± 0.11 mg TP m^{-2} day^{-1}) reported in Tipping et al. (2014). The deposition rates were the nearest available but introduce uncertainty, considering that rates can vary due to impacts of wildfires, prevailing winds and sources (Boehme et al. 2011). However, given that atmospheric deposition accounted for less than 3% of the total load in all years (see Sect. 2.3), the uncertainty introduced to P budget estimates was considered minimal. Rates were multiplied by lake surface area to calculate the daily atmospheric TP load, depending on the form of deposition determined from precipitation data. P inputs from groundwater were considered negligible, as groundwater flows contributes less than < 0.3% of the total inflow (Richerson et al. 1994). Wastewater effluent from the large population centers along the southern, eastern, and northern shores is collected and exported outside the watershed via a pipeline. Therefore, it was also assumed that the nutrient loads from wastewater would be minimal. P outputs to Cache Creek were calculated from outflow discharge volume. Streamflow data were obtained from the US Geological Survey (USGS) Cache Creek Rumsey gauge (USGS site 11451800), located ~20 miles downstream from the Clear Lake outlet. No water quality data were collected from this stream, so outflow TP concentrations were assumed to be equivalent to LA surface concentrations.

Mass balance models of internal loading

We compared watershed and atmospheric TP loads against two estimates of internal P loading to determine the relative contributions of external and internal P loading to Clear Lake's P budget. The terminology of Nürnberg (2009a, b) is used for consistency with the published literature. All internal loads are presented as areal annual loading rates (mg m^{-2} year^{-1}) to enable comparison between sub-basins.

Method 1: in situ increase in water column phosphorus

The net total and dissolved internal loads (L_{int_1}) were calculated as the observed increase within the water column during the dry season (May–October) of TP and SRP, respectively, with Eq. 2.

$$L_{int\_1} = \frac{\left(P_{t_2} \times V_{t_2}\right)}{A_{o_2}} - \frac{\left(P_{t_1} \times V_{t_1}\right)}{A_{o_1}} \tag{2}$$

Here, t_1 and t_2 are the dates of the annual minimum and maximum water column TP and SRP concentrations,

respectively, P_t is the corresponding depth-averaged P concentration through the entire water column, V_t is basin volume (m^3), and A_o is basin surface area (km^2). Hydro-acoustic survey data (ReMetrix 2003) were used in conjunction with the USGS Clear Lake level gauge at Lakeport (USGS site 11450000) to determine basin surface areas and volumes at a daily time step. Lake-wide loading rates were calculated from a surface area-weighted average of the three arms. L_{int_1} yields a net estimate, integrating both inputs and losses to sedimentation and biotic uptake. While external loading was excluded in this method, most of Clear Lake's tributaries are seasonal, diminishing to a trickle during the dry season, and are not expected to impact loading estimates.

Method 2: modeled SRP flux from anoxic sediments

Modeled estimates of gross internal P loading released from anoxic lake sediments (L_{int_2}) were quantified as the product of two component terms: days of active anoxic sediments (AA) presented in units of days per year that an entire basin's surface area is actively releasing P, and areal sediment P release rate (RR) (Eq. 3, Nürnberg 2009a, b).

$$L_{int\_2} = AA \times RR \tag{3}$$

AA was directly estimated as the number of days that deepest near-sediment DO logger in the water of each arm recorded hypoxic conditions (AA_{obs}). When the hypolimnion is hypoxic, underlying sediments can become completely anoxic and release P into the water column (Eimers and Winter 2005; Nürnberg et al. 2013a, b), as microbial-mediated sediment anoxia does not require anoxia in the overlying water column (Holdren and Armstrong 1980). Since the specific hypolimnetic DO threshold for which underlying sediment will become anoxic is not well defined, we calibrated the hypoxic threshold indicating elevated P release by comparing observed DO measurements against AA_{mod}, modeled from a log-linear regression previously applied to quantify hypoxia in polymictic systems (Eq. 4, Nürnberg 1996).

$$AA_{mod} = -36.2 + 50.1 \log \left(TP_{Jun-Oct} \right) + 0.762 \frac{Z_{mean}}{Ao^{0.5}} \tag{4}$$

Here, $TP_{Jun-Oct}$ is the June to October volume-averaged TP concentration for each lake basin, and $Z_{mean}/A_o^{0.5}$ is the basin morphometric factor with Z_{mean} in units of m and A_o in km^2. A hypoxic threshold of 3.5 mg L^{-1} was selected to calculated AA_{obs}, as this level minimized the error between modeled and observed hypoxic days (root-mean-square error [RMSE] = 10.9 days). While this threshold for redox-dependent P flux is higher than employed in many internal P loading studies, elevated deep-water TP concentrations have been observed at this DO concentration in comparable

eutrophic polymictic systems (e.g., Lake Simcoe, Eimers and Winter 2005; Nürnberg et al. 2013a, b).

Empirically derived sediment P flux rates

Arm-specific sediment SRP flux rates (RR_{core}) were quantified via incubation of quadruplicate sediment cores collected from all monitoring sites in November 2019. Samples were collected with a large-bore gravity corer from Aquatic Research Instruments fitted with polycarbonate core tubes (length 0.5 m; diameter 9.5 cm) and stored on ice during transport. Each core contained 15–25 cm of sediment and 25–35 cm of overlying water. To standardize within-site initial conditions, overlying water for each core set was siphoned off, filtered through a 0.45 μm membrane, and homogenized within a large carboy before being pumped back. Two duplicate cores were incubated under anoxic conditions, maintained by bubbling with nitrogen gas balanced with 350 ppm CO_2 for pH buffering (Moore et al. 1998; Ogdahl et al. 2014), and the remaining two were incubated under oxic conditions by bubbling with air. All incubations were maintained at a constant temperature of 15 °C and sampled approximately every 3 days for a 30-day period. Loading rates were calculated at an hourly time step by applying either oxic or anoxic release rates to the entire surface area of each arm based on observed hypolimnion DO concentrations. To account for the temperature dependence of reaction rates, fluxes were modified by van 't Hoff's Q_{10} rule of 3 (i.e., a 10 °C temperature increase corresponds to a tripling of the P flux rate, Eq. 5). This Q_{10} coefficient has been widely used to model temperature effects of diffusive P fluxes (Liikanen et al. 2002; Nürnberg 2009a, b).

$$RR_{Temp} = RR_{core} \times Q_{10}^{(ti-15)/10} \tag{5}$$

Here, RR_{Temp} is the average hourly P flux rate based on the deviation of the observed sub-basin hypolimnetic temperature from the incubation temperature (t_i − 15) and $Q_{10} = 3$.

Experimentally determined RR values were compared against two other modeled RR estimates derived from water column and sediment TP concentrations. In a study of anoxic incubated sediment cores from 17 reservoirs across the US central plains, Carter and Dzialowski (2012) found that RR values were significantly correlated with trophic status and TP concentration in the water column and developed a log-linear model to predict RR from summer TP concentrations (Eq. 6, $R^2 = 0.37$, $p = 0.009$, $n = 17$).

$$\log(RR_{TP}) = -0.540 + 0.827 \log \left(TP_{Jun-Oct} \right) \tag{6}$$

Here, $TP_{Jun-Oct}$ is the depth-averaged TP concentration in the photic zone. Unlike the original study, we chose to use the average TP concentration throughout the water column,

since intermittent mixing facilitates consistent vertical nutrient transport in Clear Lake throughout the summer. RR values are also correlated to sediment P composition (Nürnberg 1988) and can be estimated via a regression with sediment TP concentration (Eq. 7, $R^2 = 0.21$, $p < 0.001$, $n = 63$).

$$\log(RR_{sed}) = 0.8 + 0.76 \log\left(TP_{sed}\right) \tag{7}$$

Here, TP_{sed} is the average concentration of TP in the upper 5 cm of lake sediment in mg g^{-1} of dry weight. Sediment TP concentrations were measured from oxic incubation cores following the November 2019 incubation.

Stratification metrics

The timing of stratification events was determined based on the mean hour Brunt–Väisälä buoyancy frequency in the water column ($\overline{N}[s^{-1}]$). We assumed Clear Lake was thermally stratified when $\overline{N} > 0.015$ s^{-1}, a threshold previously determined by Cortés et al. (2021).

Statistical analyses

Ordinary least squares regression analyses between explanatory environmental factors (nutrient concentrations, daily average surface water temperature, and 3-day trailing average wind speed/DO) with cyanobacteria biovolume were performed in MATLAB to determine which set of parameters predicted the greatest variation in cyanobacteria intensity (CI). A Box–Cox transformation (*boxcox* MATLAB® function) was applied to each dataset to ensure normal distribution. Spearman rank correlations were initially calculated to assess the strength and direction of the association between each predictor variable and cyanobacteria response. A minimum redundancy–maximum relevance (MRMR) algorithm (*fsmrmr* MATLAB® function) was then applied to rank the importance of each predictor and determine the appropriate number of predictor variables to include in a regression. MRMR is a two-stage feature selection algorithm that finds the optimal set of predictors that are mutually and maximally dissimilar and can represent the response variable effectively (Peng et al. 2005). The algorithm first calculates the relevance of each predictor, based on the mutual information metric, and then calculates the redundancy between each predictor pair. Predictors are then ranked by subtracting redundancy from relevance. The optimal multiple linear regression model was then selected based on the adjusted R^2 and the Bayesian information criteria (BIC).

To assess the strength of long-term and seasonal trends in HCB intensity, the time series of spatially averaged CI for each basin and the entire lake was decomposed (*trenddcomp* MATLAB function) into additive long-term trend (LT), seasonal trend (ST) and residual (R) components such that the

observed $CI = LT + ST + R$. The strength of the long-term trend (F_T) and seasonality (F_s) between 0 and 1 was evaluated via Eqs. 8 and 9 (Wang et al. 2006):

$$F_T = \max\left(0, 1 - \frac{\text{Var}(R)}{\text{Var}(LT + R)}\right) \tag{8}$$

$$F_S = \max\left(0, 1 - \frac{\text{Var}(R)}{\text{Var}(ST + R)}\right) \tag{9}$$

Results

Spatial and temporal variability of stratification and hypoxia

Thermistor chains recorded multiple intermittent cycles of thermal stratification and mixing from March to November each year with stratification periods ranging from daily to monthly timescales (Online Resource Figs. S.3–S.5), surface temperatures ranging from 22 to 29 °C, and vertical temperature differences exceeding 6 °C during the summertime. Within a week of stratification onset, hypolimnetic DO concentrations rapidly declined to anoxic levels due to high oxygen demand in the hypolimnion, but the timing and duration of these events differed in each of the three summers (Table 2). In 2019, the lake was more consistently anoxic during May and June (31% of the time) than in 2020 (5%) or 2021 (12%). In contrast, the lake was less anoxic in July and August 2019 (37%) than in 2020 (45%) or in 2021 (73%). Similarly, anoxia rarely occurred in September and October 2019 (1%) but was more frequently observed in 2020 (15%) and 2021 (10%). Although the earliest anoxic period was

Table 2 Annual totals of observed hypoxic days in the hypolimnion Upper (average of three monitoring sites), Oaks (OA-04), and Lower (LA-03) Arms at three DO thresholds and the modeled active sediment area factor (equation 4, AA$_{mod}$)

		2019	2020	2021
Upper (average)	HDO < = 1 mg L^{-1}	28	39	49
	HDO < = 2 mg L^{-1}	61	56	61
	HDO < = 3.5 mg L^{-1}	88	93	88
	AA$_{mod}$	84	93	101
Oaks	HDO < = 1 mg L^{-1}	25	37	41
	HDO < = 2 mg L^{-1}	39	52	56
	HDO < = 3.5 mg L^{-1}	73	77	91
	AA$_{mod}$	78	88	95
Lower	HDO < = 1 mg L^{-1}	23	24	37
	HDO < = 2 mg L^{-1}	35	36	50
	HDO < = 3.5 mg L^{-1}	59	71	82
	AA$_{mod}$	82	92	99

observed in April 2019, the cumulative duration of anoxia and hypoxia increased across all arms each subsequent year of the study (Fig. 2). In 2020 and 2021, the lake remained continuously thermally stratified throughout much of the mid-summer, resulting in multi-week hypoxic periods in all three arms in July and August.

Clear Lake's spatially variable wind field drove interbasin variability in the duration of summertime stratification and hypoxia. Winds blow predominantly along a northwesterly axis, and the orographic effect of Mount Konocti focuses winds through the Oaks and Lower arms resulting in higher wind speeds in the eastern side of the lake relative to the west (Rueda et al. 2008). As a result, the UA experienced longer periods of stratification and hypoxia than the other two arms, despite its comparatively shallow depth. A frequency distribution of summertime wind speeds highlights the interbasin variability in wind forcing (Online Resource Fig. S.9). In the UA, summer winds averaged between 0.81 and 0.98 ms^{-1} and rarely exceeded 5 ms^{-1}, while winds in the two eastern arms averaged between 1.30 and 3.02 ms^{-1}, with gusts up to 10 ms^{-1}. These stronger winds provided more mechanical energy to the eastern two arms, frequently eroding the thermocline of these arms days before the UA mixed. For example, at the end of stratification periods in August 2020 and 2021, $\overline{N}$ in the UA remained above the 0.015 s^{-1} stratification threshold for 3 and 5 days longer, respectively, than in the other two arms (Fig. 3).
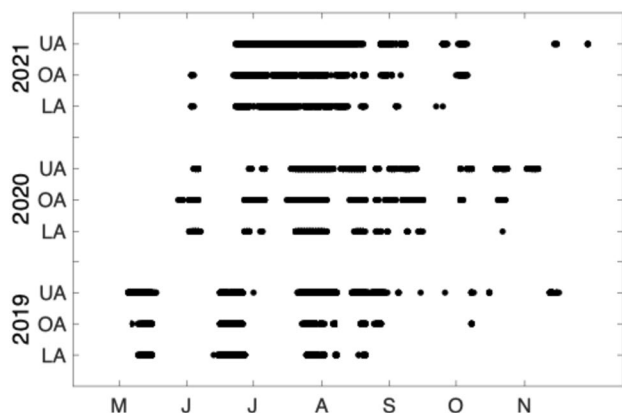

Fig. 2 Timing of hypolimnetic anoxia across Clear Lake sub-basins. Black dots indicate periods when hourly DO < 1 mg L^{-1}
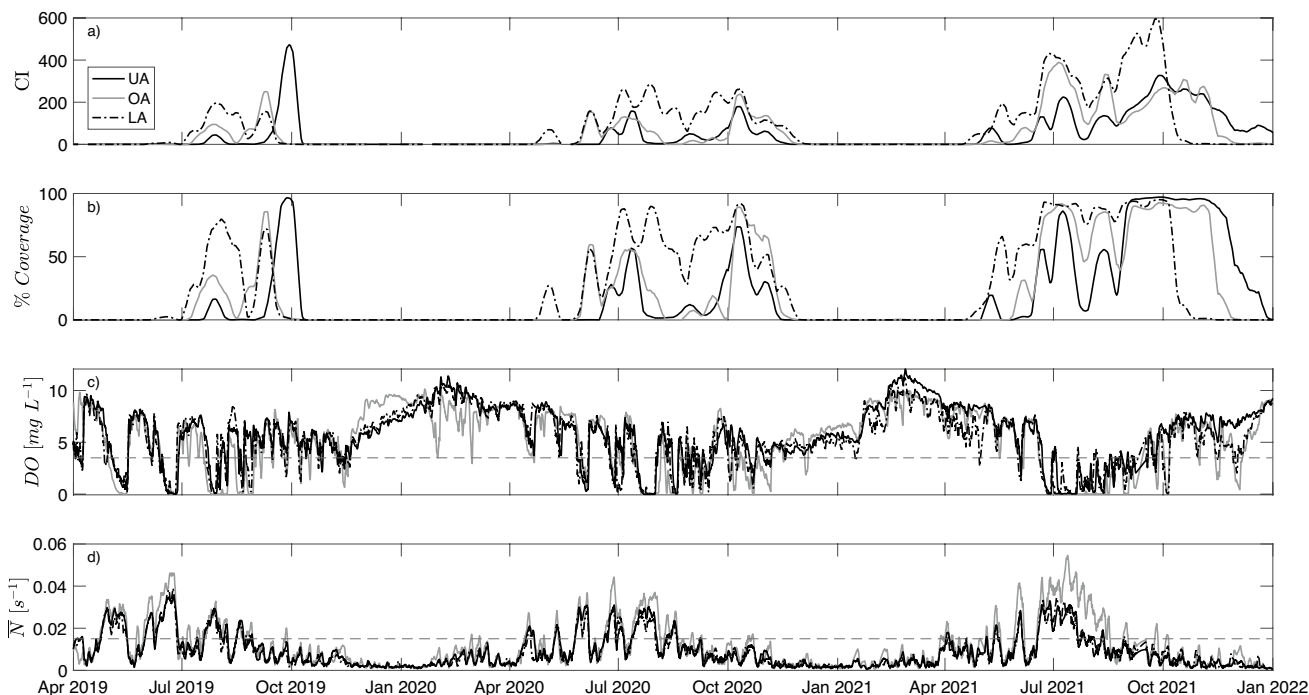

Fig. 3 a Spatially averaged, 7-day moving average of the trailing 10-day maximum modified cyanobacteria index Upper (dark gray), Oaks (light gray), and Lower (black) arms. b Percent coverage of cyanobacteria of arm surface area. c DO measured at 0.5 m above sediment–water interface at deepest point in each arm. The dashed line indicates the 3.5 mg L^{-1} hypoxia threshold. d Average buoyancy frequency in the water column. The dotted line indicates the threshold for stratification at $\overline{N} = 0.015$ s^{-1} (2019–2021).

Seasonal nutrient variability

Lake-wide TP concentrations followed a consistent seasonal pattern in all three arms, with annual minimums observed each spring (< 0.05 mg L^{-1}), increasing throughout the summer and peaking in early fall (Fig. 4). The annual peak concentrations were observed simultaneously in all three arms, with the highest concentrations occurring in the UA (0.5–0.8 mg L^{-1}) during September 2019 as well as in October 2020 and 2021. The maximum concentrations in the deeper OA and LA sites were comparatively lower, ranging from 0.3 to 0.7 mg L^{-1}.

The summer TP increase was primarily comprised of SRP, which accounted for 75–95% of TP in the water column from July to October. Elevated TP and SRP concentrations in the hypolimnion in early summer preceded increases in the epilimnion in early fall. Average TN concentrations followed a similar seasonal pattern with annual minimums in the spring (~0.35 mg L^{-1}), increasing throughout the summer and reaching a peak in the fall/winter (0.5–1.1 mg L^{-1}). TN was significantly correlated with TP ($r = 0.59$, $p < 0.001$). NH$_4$, measured from March 2020 onwards, was higher in the summer and fall (0.125 mg L^{-1}) than in winter and spring (~0.002 mg L^{-1})
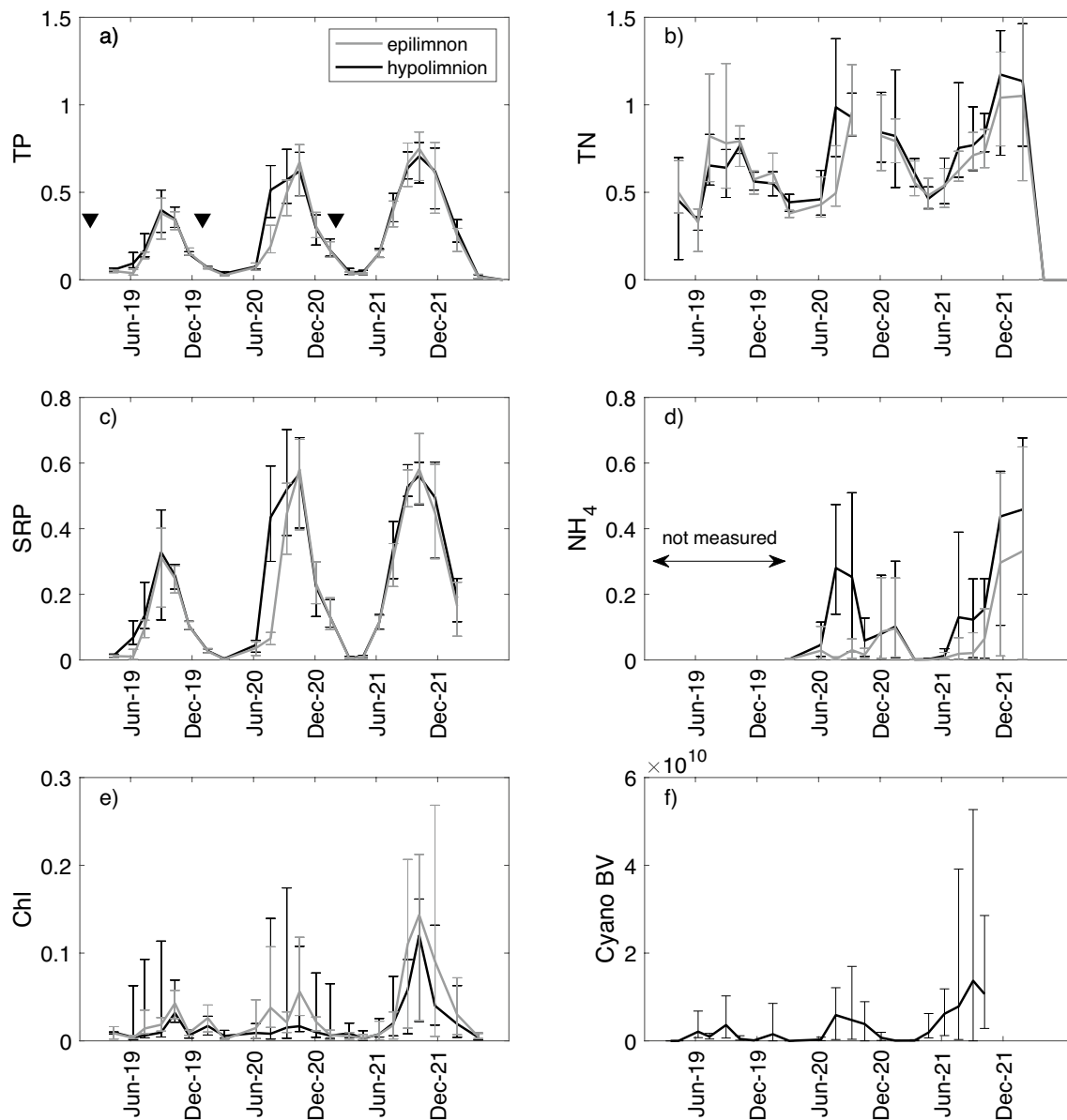

Fig. 4 Mass of **a** total phosphorus, **b** total nitrogen, **c** soluble reactive phosphorus, **d** ammonium, and **e** chlorophyll-a in the epilimnion (gray) and hypolimnion (black) averaged across all monitoring sites [mg L^{-1}]; **f** biovolume of cyanobacteria in surface samples [μm^3 L^{-1}]. Black arrows indicate the timing of maximum external loading input. Error bars indicate the range of values measured across all sites

with the highest concentrations observed in the LA and the OA. Like SRP, NH_4 concentrations increased sharply near the lakebed during the summer, indicating internal N release. In contrast, $NO_2–NO_3$ concentrations were higher in the fall and winter (0.08–0.14 mg L^{-1}) and lower (0.001 mg L^{-1}) during spring and summer, suggesting that algal uptake and denitrification was occurring during stratification. The seasonality of NH_4 and $NO_2–NO_3$ accounts for the variability in TN. In addition, external loading of N following winter storms likely contributed to higher wintertime TN concentrations.

External loads

Total external areal TP loads from the watershed to Clear Lake during 2019, 2020, and 2021 were 72, 40, and 80 mg TP m^{-2}, respectively, while areal TP loads from atmospheric deposition (L_{atm}) were 78, 84, and 80 mg TP m^{-2} in each respective year (Table 3). The interannual variation in L_{ext} resulted from the extreme variability in the region's precipitation, with 2019 being a wetter-than-average year, while 2020 and 2021 were two of the driest years on record (Fig. 5a). External TP inputs from tributaries are primarily conveyed to the UA (> 90% of watershed inflows) and varied seasonally. External loads were greatest during the

Table 3 Comparison of external watershed (L_{ext}) and internal loading estimates for Clear Lake and sub-basins (2019–2021)

Year	L_{ext}	L_{atm}	Basin	L_{int_1} TP	L_{int_1} SRP	$L_{int\_2\_Core}$ RR_{temp}	$L_{int\_2\_TP}$ RR_{TP}	TMDL
2019	721	78	UA	2830	2690	1770	2900	548
			OA	2550	2400	2950	1810	
			LA	1960	1590	2020	1350	
			Clear Lake	2630	2440	1960	2500	
2020	40	84	UA	3840	3840	2300	4510	
			OA	4120	3860	4640	2780	
			LA	3540	3320	3350	2270	
			Clear Lake	3800	3740	2810	3910	
2021	80	80	UA	3790	3110	2290	4780	
			OA	4680	4140	5440	4060	
			LA	3730	3510	4820	3240	
			Clear Lake	3860	3280	3240	4400	

All load estimates are presented as areal rates in mg TP m^{-2} $year^{-1}$. Clear Lake nutrient TMDL is shown in the right column for comparison
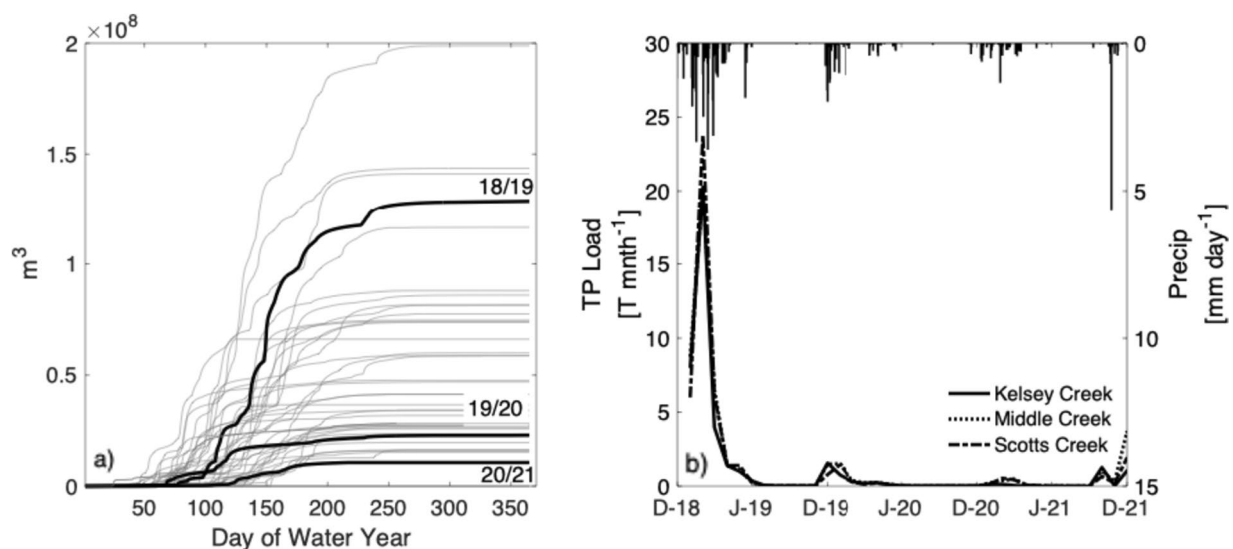

Fig. 5 **a** Water year (i.e., Oct 1–Sept 31) cumulative discharge from Middle Creek from 1980 to 2022. Water years from Oct 2018 to Sept 2022 are shown in bold. **b** Monthly TP load estimates from gauged Clear Lake tributaries and precipitation data measured

winter (October–March), declined throughout the spring, and reached near zero during the summer.

Internal loads

In situ increase in water column phosphorus (L_{int_1})

Net lake-wide, annual, and internal TP loading estimates derived from water column measurements were 2630, 3800, and 3860 mg TP m^{-2} in 2019, 2020, and 2021, respectively, with more than 40% variation in loading rates observed between arms (Table 3). L_{int_1} estimates for SRP fluxes were similar in magnitude with rates of 2440, 3740, and 3280 mg SRP m^{-2} during each respective summer. The timings of the TP and SRP internal loads were consistent with one another. The lowest areal loading rates consistently occurred in the LA, while the highest rates were observed in the UA in 2019 and in the OA in 2020 and 2021. Despite lower observed TP concentrations in the OA, its surface area is 88% smaller than the UA, resulting in comparative areal release rates between the two arms.

Modeled P flux from anoxic sediments (L_{int_2})

Mean estimates for basin-specific anoxic sediment SRP release rates in incubations ranged from 10.5 to 24.6 mg SRP m^{-2} day^{-1}, while oxic release rates were an order of magnitude smaller, ranging from 0.17 to 0.6 mg SRP day^{-1} (Table 4). Release rates from the UA ranged from 8.8 ± 0.09 (UA-08) to 11.6 ± 0.94 mg m^{-2} day^{-1} (UA-01) and were more than 50% lower than those observed in the Narrows (26.7 ± 3.86 mg m^{-2} day^{-1}), the OA (24.9 ± 0.86 mg m^{-2} day^{-1}), or in the LA (21.4 ± 1.61 mg m^{-2} day^{-1}). RR rates calculated from sediment TP concentrations (RR$_{sed}$) were significantly lower than observed in lab incubations and ranged from 6.1 to 7.9 mg m^{-2} day^{-1}, while fluxes modeled

Table 4 Comparison of estimated sediment P release rates (mg TP m^{-2} day^{-1})

Method	UA (mean)	OA	LA
Oxic RR$_{core}$	0.17	0.55	0.61
Anoxic RR$_{core}$	10.5	24.6	21.4
RR$_{sed}$	6.1	6.1	7.9
RR$_{TP\_2019}$	30.9	25.7	22.9
RR$_{TP\_2020}$	45.0	38.1	34.1
RR$_{TP\_2021}$	54.4	44.6	39.5

RR$_{core}$ is the average SRP diffusive flux measured in duplicate oxic and anoxic sediment cores. RR$_{sed}$ is the TP release rate modeled from linear regression with TP concentration in the upper 5 cm sediment of duplicate oxic cores. RR$_{TP}$ is the TP release rate modeled from linear regression with average summer TP concentration through the water column for each study year.

from lake summertime TP concentrations (i.e., RR$_{TP}$) ranged from 22.9 to 30.9 mg TP m^{-2} day^{-1} in 2019, 34.1 to 45.0 mg TP m^{-2} day^{-1} in 2020, and 39.5–54.4 mg TP m^{-2} day^{-1} in 2021 across arms. RR$_{TP}$ estimates in 2019 were consistent with RR$_{core}$ estimates for the OA and the LA but predicted a substantially larger RR in the UA than was experimentally determined.

The lake-wide gross internal SRP loads estimated from the incubation release rates ($L_{int\_2\_core}$) were 1960, 2810, and 3240 mg SRP m^{-2} year^{-1} in 2019, 2020, and 2021, respectively. Modeled internal TP load estimates utilizing RR$_{TP}$ ($L_{int\_2\_TP}$) were 28–36% larger than predicted by core incubation: 2500, 3910, and 4400 mg TP m^{-2} year^{-1} in 2019, 2020, and 2021, respectively. Greater loading rates predicted from RR$_{TP}$ were due to higher predicted sediment flux rates in the UA.

Cyanobacteria temporal and spatial variability

Satellite imagery recorded two peaks in cyanobacteria biomass in Clear Lake each summer, though there was significant interannual variability in the timing and intensity of the HCB season (Fig. 3, Online Resource Fig. S.6). The bloom magnitude (BM) metric indicated that the HCB was increasingly intense each summer (BM = 8115, 16,848, and 37,572 in 2019, 2020, and 2021, respectively. Time series decomposition of the *CI* time series further demonstrated that there was a strong long-term increasing trend in the HCB intensity across all three arms (F_T = 0.56, 0.58, 0.60 in the UA, OA, and LA, respectively, Online Resource Fig. S.11).

In 2019, following a particularly wet winter, the spatial extent of the bloom was relatively small, with large patches only detected from July through early October in each arm; peak cyanobacteria biovolumes occured in late August. An early summer bloom began forming in the LA on July 4, 2019, following a 12-day stratified period and subsequent mixing event on June 26. The LA bloom increased in size from July 18 to 31, while the lake remained thermally stratified, reaching a maximum extent of 80% of the arm's surface area on July 31 before declining through mid-August following a mixing event on August 1, indicated by a decreasing $\overline{N}$ and a sudden increase in bottom DO. A subsequent fall bloom began forming in the OA and the LA on August 22, shifting to the UA 2 weeks later on September 10. The fall bloom continued to grow, reaching a spatial coverage of 97% of the UA's surface in late September, while water temperatures declined, and the lake became increasingly well mixed. The fall bloom rapidly declined from its peak on September 28, covering less than 2% of the UA surface by October 8.

In 2020, blooms began to form in the LA and the OA on May 30 during a stratification period that lasted from

May 26 to June 5. This bloom, only observed in the two smaller arms, reached a peak on June 4 (~ 50% coverage) and began to decrease in size following a mixing event on June 6. Blooms were detected in all three arms on June 18, growing in extent until July 15 before declining to near levels in the OA and the UA by August 8 and in the LA by August 26. Unlike the previous summer, this decline occurred while they lake was stably stratified from July 17 to August 1. From August 26 to October 5, blooms began to proliferate in all three arms, covering ~ 85% of the lake by early October. As in 2019, the blooms continued to grow through the early fall despite decreasing lake stability. The 2020 fall bloom declined slowly from its peak, continuing to cover at least 50% of the OA and the LA through early November. Peak cyanobacteria biovolumes for the 2020 season were observed in late July samples in the UA and in September in the OA and the LA.

The 2021 bloom season was the most severe observed during the monitoring period. Blooms in the LA started to form in late April prior to the onset of stratification. From June 13 to July 29, blooms began to grow in extent across all three arms, covering nearly 90% of each arm at its peak, while the lake remained predominantly stratified, and hypolimnetic DO concentrations were consistently < 1 mg L^{-1}. This early summer bloom decreased in intensity in all three arms from July 13 to 29 but continued to cover more than 60% of the LA. Blooms began to rebound in all three arms on August 1 and increased in coverage throughout August until ~ 92% of the lake was covered on August 31. This late summer bloom continued covering the majority of the lake until October 8 when the bloom disappeared from the surface of the LA, followed by a declined in the OA a month later on November 11. A bloom continued to wain in the UA but persisted until January 2022. The highest cyanobacteria biovolumes detected in 2021 were observed in the LA on July 22, in the OA on September 3, and in the UA on October 7. Despite interannual variation in intensity, the blooms followed an analogous bimodal seasonal evolution with peaks in bloom coverage in early summer and fall separated by a mid-summer minimum. The seasonal component of the *CI* time series showed the strongest seasonal trend in the LA ($F_S = 0.53$), while the strength of the seasonal trend in the OA ($F_S = 0.38$) and UA ($F_S = 0.28$) was weaker (Online Resource Fig. S.11). The early summer peak was most prevalent in the LA, while the fall peak was primarily observed in the UA.

Spatial and temporal variation in cyanobacteria community composition highlights the complexity of Clear Lake's phytoplankton ecology (Fig. 6). During each summer, the early season peak was dominated by N-fixing cyanobacteria, while the fall peak contained both N-fixing and non-N-fixing genera. In summer 2019, *Aphanizomenon* and *Dolichospermum* dominated from June to August, comprising 22–92% of

the total cyanobacteria biovolume. In comparison, in 2020, the early summer peak was dominated by *Gloeotrichia* and *Dolichospermum*, while *Aphanizomenon*, *Limnoraphis*, and *Dolichospermum* dominated in June and July of 2021. In contrast, non-N-fixing *Microcystis* and *Pseudanabaena* were observed in September and October. *Microcystis* was predominantly observed in the LA, the OA and the Narrows. Unlike other genera, *Microcystis* cannot fix nitrogen and must utilize in-lake sources of N. Since bioavailable nitrate and nitrite concentrations are very low in the summer due to denitrification and algal uptake, this genus tends to form where there is available NH_4, such as the OA and the LA. The interbasin variability in cyanobacteria ecosystem composition highlights the spatial heterogeneity of cyanobacteria blooms across Clear Lake's three arms.

Drivers of cyanobacterial blooms

Table 5 details the Spearman rank correlations between environmental predictor variables and cyanobacteria biovolume for 116 samples collected throughout the entire year from 2019 to 2021. Significant and positive correlations were observed between surface temperature ($\rho = 0.53$, $p < 0.001$), TP ($\rho = 0.52$, $p < 0.001$), and TN ($\rho = 0.48$, $p < 0.001$), while TN:TP was negatively correlated ($\rho = -0.40$, $p < 0.001$). No significant correlations were observed between DO, Chla, or wind speed with biovolume. The rank of each predictor variable, based on the MRMR algorithm, indicated that TN:TP and water temperature were the two most important predictors (Fig. 7), followed by DO, TP, and TN. The drop in importance score between each term represents the confidence of feature selection. While there was a large decrease in the importance score after the first two terms, the decrease in score for subsequent predictors was relatively small, implying that the difference in predictor importance for these latter terms was not significant. A linear model incorporating both TN:TP and water temperature explained 43% of the variance in cyanobacteria biovolume (Table 6). Adding an additional DO term improved the adjusted R^2 of the model to 0.45; however, the BIC of the three-parameter model also increased, indicating that a multiple linear regression using only TN:TP and water temperature is preferred, as it provides a simpler and more parsimonious explanation of the data.

Discussion

Clear Lake's morphometry (i.e., its shallow depth and large surface area-to-volume ratio), warm in-lake summer temperatures, and high rates of primary production make the system conducive to internal P loading. In this study we hypothesized that (1) diffusive P fluxes from anoxic sediments were the
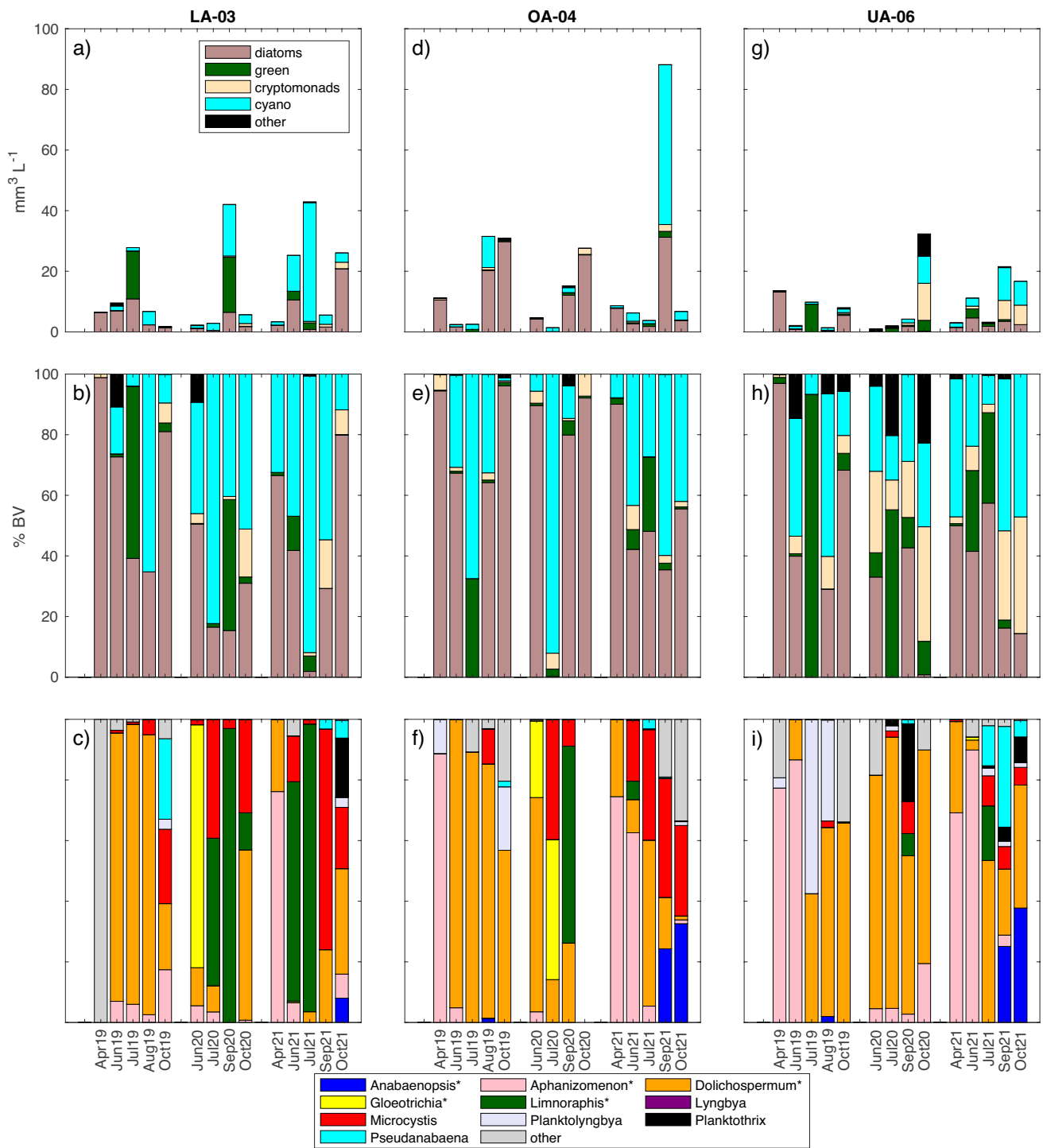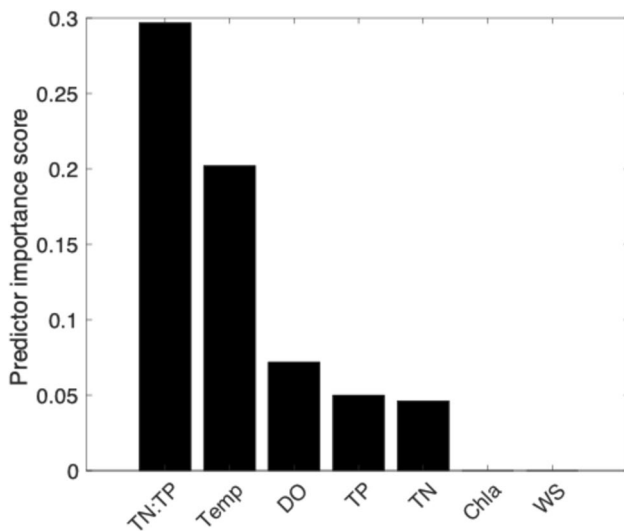
Fig. 6 **a–c** Total and **d–f** proportional biovolume for major phytoplankton groups and **g–i** proportional biovolume of major cyanobacteria genera across sub-basins from April to October (2019–2021). The asterisk indicates N-fixing species

Table 5 Spearman rank correlation coefficients for biovolumes of total cyanobacteria and selected cyanobacteria genera with environmental parameters measured in the water column, surface water temperature (Temp), bottom water DO (DO), and 3-day trailing wind speed (WS). 2019–2021 ($n = 116$). Correlations with $p < 0.001$ are bolded

	Chla	TP	TN	TNTP	Temp	DO	WS
cyano	0.25	**0.52**	**0.48**	**−0.40**	**0.53**	−0.22	0.26
micro	0.24	**0.38**	0.27	**−0.30**	0.21	−0.01	−0.07
anab	0.04	0.06	0.02	−0.07	0.14	0.06	0.15
lyng	−0.10	0.07	0.02	−0.09	0.10	**−0.37**	0.09
doli	**0.30**	**0.51**	0.27	**−0.48**	**0.79**	−0.28	0.29
gloeo	0.03	0.03	0.06	0.01	0.25	−0.19	0.27

Correlations with $p < 0.001$ are bolded

Fig. 7 Predictor rank calculated from MRMR algorithm

Table 7 Internal and external TP load estimates (metric tons) for January–December (2019–2021)

Year	Internal TP load	External TP load	Internal load contribution (% total)
2019	412 (306)	130	70 (59)
2020	605 (432)	22	96 (95)
2021	597 (492)	27	97(95)

primary source of phosphorus loading to Clear Lake, (2) internal P loading created an *N*-limiting environment during the summer, promoting blooms of nitrogen-fixing cyanobacteria, and (3) annual variation in the timing and duration of hypoxia regulated the magnitude of the summer HCB season. During the 3-year monitoring period, we observed large increases in lake TP each summer, which were an order of magnitude larger than watershed P inputs from preceding winters with internal sources accounting for 70%, 97%, and 96% of the total TP load in 2019, 2020, and 2021, respectively (Table 7). Moreover, the largest increases in the water column TP occurred in the late summer and early fall each year, when external loading from tributaries was lowest, further

supporting hypothesis (1). Nutrient measurements and phytoplankton identifications corroborated hypothesis (2), indicating that increased summertime TP lowered the N:P ratio below the 16:1 Redfield ratio, shifting the nutrient limitation from P to N (Fig. 8). While the largest wintertime external TP loading occurred prior to summer 2019, the highest peak in-lake TP concentrations were observed in 2021, resulting in the most severe HCB season recorded since 2004 (Fig. 9). Through our high-frequency measurements of temperature and oxygen, we demonstrated the validity of hypothesis (3) attributing the high concentrations of TP observed in 2021 to warmer air temperatures, prolonged periods of stratification, and resultant hypolimnetic hypoxia that persisted throughout the summer. The following sections will provide further supporting evidence for each of these hypotheses. While many eutrophic lakes that experience regular HCBs have high internal P loading rates due to oxygen depletion at the sediment–water interface (SWI) and high rates of organic matter production (Søndergaard et al. 2001; Spears et al. 2012), it is rare for it to dominate P cycling to such a large extent.

Internal load estimates are based on the observed increase in water column TP (L_{int_1}). Internal load estimates

Table 6 Comparison of multiple linear regression models for predicting cyanobacteria biovolume

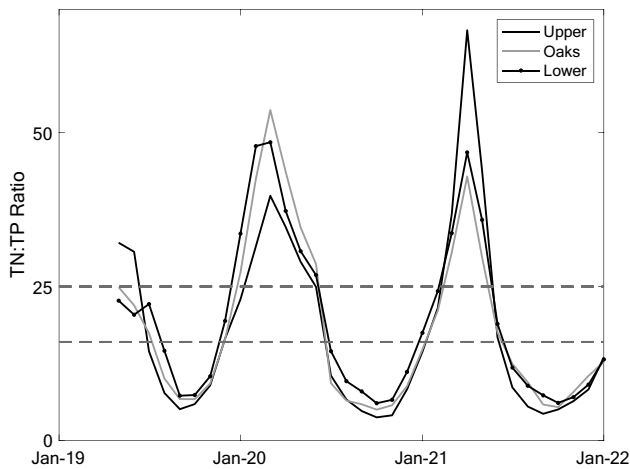| Model	R^2	Adj. R^2	p	BIC
log(cyano bv) = 252.8 − 39.4 log(TNTP)	0.26	0.25	< 0.001	1258
log(cyano bv) = −89.4 + 96.0 log(Temp) − 16.1 log(TNTP)	0.46	0.43	< 0.001	1226
log(cyano bv) = −82.4 + 94.9 log(Temp) − 14.9 log(TNTP) − 3.76 log(DO)	0.46	0.45	< 0.001	1231

Fig. 8 Volume-averaged TN:TP molar ratios for each sub-basin. Dotted lines indicate 25:1 (Maranger, 2018) and 16:1 (Redfield 1958) thresholds
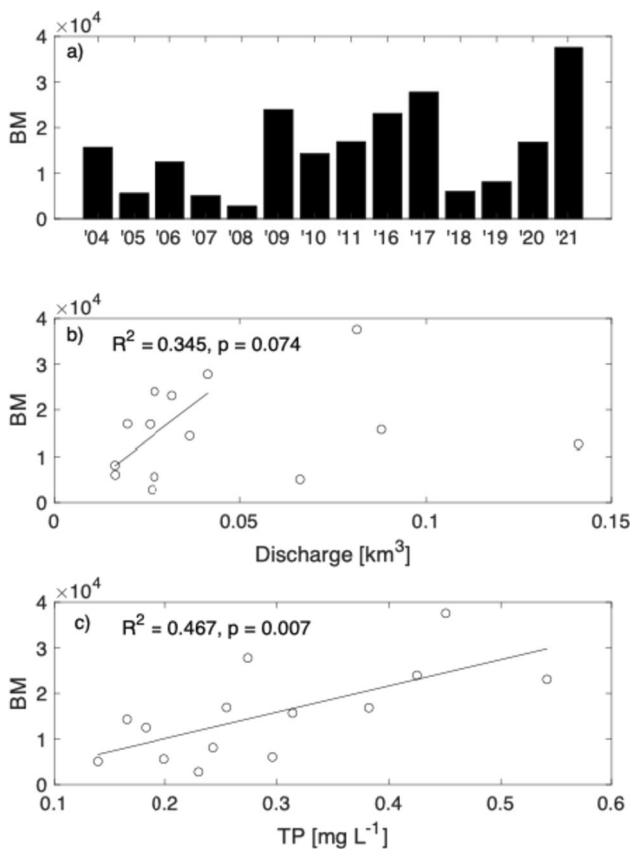

Fig. 9 a Seasonal cyanobacteria bloom magnitude (June–October) recorded by satellite imagery from 2004 to 2011 and 2016 to 2021. No satellite data were available from 2012 to 2015. Scatter plots comparing **b** cumulative inflow from previous water year vs. bloom magnitude and **c** average summer TP concentration vs. bloom magnitude

calculated from experimentally determined releases rates are shown in parentheses. External load is the sum of both watershed and atmospheric contributions

Contribution of external and internal loading

While TP loads from the watershed were greatest during the wet winter season, the highest water column TP concentrations were observed during each summer and fall, demonstrating the prevalence of internal P loading in the system. In summer 2019 and 2020, TP increased in the hypolimnion faster than in the epilimnion, further indicating that the sediments acted as a major internal source of TP. By subtracting external load contributions from the observed increase in water column TP during the dry season (i.e., $L_{\text{int\_}1}$), we determined that internal sources accounted for more than 70% of the TP in the lake each summer (Table 7). While atmospheric load estimates varied interannually by less than 10%, watershed loads were significantly less in 2020 and 2021 due to lower-than-average stream inputs as a result of a prolonged drought, resulting in a higher relative contribution of internal loading to the overall P budget. The overwhelming influence of internal loadings on P cycling in Clear Lake suggests that focusing on managing in-lake internal P sources (e.g., dredging, hypolimnetic oxygenation, alum application) is more likely to result in improved water quality than focusing on non-point source pollution from the watershed (De Palma-Dow et al. 2022). Nevertheless, lake restoration requires a holistic approach in which both external and internal sources are managed.

Contribution of internal P loading to seasonal N limitation

While many freshwater systems have been historically viewed as P-limited environments, the release of P from sediments in eutrophic systems can increase phosphorus availability in the water column, thereby reducing N:P ratios and shifting the system towards N limitation (Ding et al. 2018; Wu et al. 2020). As a result of the large mass of P released from sediment pools during hypoxic periods, Clear Lake experienced N limitation at least 8 months each year, with TN:TP molar ratios remaining consistently < 25 from June through January (Fig. 8). TN:TP was utilized to indicate nutrient limitation, rather than DIN:SRP, as TP and SRP were strongly correlated ($r = 0.98$, $p < 0.001$). Our findings align with historical monitoring data which show persistently low TN:TP ratios in Clear Lake since the early 1970s (Online Resource Fig. S.2) and with high concentrations of TP and SRP corresponding with low DO (De Palma-Dow et al. 2022). Florea (2022) likewise observed consistent N limitation across 10 Clear Lake monitoring sites in 2020 and 2021. These results agree with an analysis of 369 German lakes, which found that shallow polymictic lakes are predominantly N-limited during the summer (Dolman et al. 2016).

When ratios of N:P are low, cyanobacteria often dominate phytoplankton assemblages, as their ability to fix nitrogen provides a competitive advantage over other N-limited

groups (Smith [1983]). With the exception of *Microcystis and Pseudanabaena*, all dominant cyanobacteria genera in Clear Lake are N-fixing, allowing them to thrive in N-limited environments. The strong negative correlation between TN:TP and cyanobacteria biovolume supports our hypothesis that the relative abundance of cyanobacteria increases as the N:P ratio decreases. The MRMR predictor rank further highlights TN:TP ratio as the single most important predictor of cyanobacteria bloom intensity. The TN:TP ratio was higher ranked than either TN or TP alone, likely because the ratio incorporates both the amount of TP available to cyanobacteria and the amount of N-limiting growth of other phytoplankton groups. Thus, this statistically significant correlation provides further evidence that internal P release from lake sediment promotes the proliferation of HCBs by both increasing bioavailable limiting nutrients and altering the nutrient balance in favor of N-fixing cyanobacteria.

Seasonal and inter-annual variability of HCBs

While there was variability in the intensity and duration of each summer bloom season, there were commonalities in their temporal evolution. In each year, the bloom season could be separated into three periods: (1) an early summer bloom in June and July predominantly in the LA, when Aphanizomenon began the bloom, (2) a late summer minimum in August, and (3) a large fall bloom in September and October predominantly in the OA and the UA. This bimodal pattern corroborates the findings of Horne ([1975]) who documented a seasonal succession of cyanobacteria species in Clear Lake with peaks of *Aphanizomenon* in early summer and *Anabaena* in early fall separated by a minimum in cyanobacteria biomass in late summer. Horne hypothesized that the mid-summer decline was due to iron depletion, a trace element integral to the nitrogenase enzyme required for N fixation, limiting the growth of diazotrophs. Iron limitation on nitrogen fixation has been widely observed in both freshwater and marine systems (Hanington et al. [2016]; Mills et al. [2004]; Wurtsbaugh and Horne [1983]). Dissolved iron measurements collected from 1970 to 2020 in Clear Lake show a decrease in the monthly average and minimum concentrations from June through September, indicating that the system was likely iron-limited in the late summer (Summary Report on Metals and Metalloids in Clear Lake [2022]). Seasonal cyanobacteria succession can also be regulated by zooplankton grazing, day length, light availability, and water temperature (Abrantes et al. [2006]).

Cyanobacteria community composition data further demonstrate that the seasonal pattern in bloom intensity is a result of shift in the dominant genera. For example, during June and July of 2020, *Gloeotrichia* was detected in all monitoring sites, except for UA-06, but completely disappeared from the fall bloom, replaced by *Limnoraphis* as the dominant species in September 2020. Similarly, *Aphanizomenon*

was prevalent in April and June samples in 2021 but was succeeded by *Pseudanabaena* and *Microcystis* as the dominant genera in September 2021 samples. Neither *Pseudanabaena* nor *Microcystis* can fix nitrogen, so their appearance in the fall is likely driven by increasing availability of TN, which increased throughout the summer each year (Florea et al. [2022]).

In comparison to all bloom seasons since 2004, BM in 2019 and 2020 was below average, whereas the 2021 BM was the most severe on record (Fig. [9]). The highest cyanotoxin levels, specifically *Microcystin*, ever documented in the lake were observed August 2021, providing further evidence of the exceptional bloom magnitude in that summer (Big Valley EPA [2021]). Annual bloom magnitudes in Clear Lake show a significant, positive linear correlation with summertime TP concentrations in the lake ($R^2 = 0.47$, $p = 0.007$). However, contrary to observations from many eutrophic systems (Kane et al. [2014]), high wintertime external loading rates were not correlated with the magnitude of the subsequent HCB season. While discharge from Middle Creek was linearly correlated with BM during years with cumulative discharge less than 0.05 km^3 ($R^2 = 0.35$, $p = 0.074$), for high flow years, the relationship is nonlinear. In fact, during this 3-year study, we observed an inverse relationship to discharge, with years of low external loading corresponding to more severe blooms. This result is consistent with the observations of De Palma-Dow ([2022]), which found that summer TP concentrations in Clear Lake were negatively correlated with precipitation during the previous winter. While this study covers only three summers, we were able to observe HCB seasons following both extremely wet and extremely dry water years. Precipitation accumulations during the 2018–2019, 2019–2020, and 2020–2021 water years were respectively 170%, 55%, and 30% of the average rainfall from 1997 to 2021. While P loading from sediments is primarily driven by internal processes, TN concentrations each year were highest in the early winter following major storm events. This pattern suggests that external loading may be more important in controlling N availability than P availability and is supported by the fact that the UA, which receives the majority of stream inflows, had an N:P ratio < 20 in July 2019 but dropped below this threshold a month earlier in both 2020 and 2021 when inflows during the previous winters were low (Fig. [8]).

In contrast to external loading, we observed that the timing and duration of stratification events, resulting from variability in summer meteorological conditions, strongly influenced in-lake TP concentrations and the severity of the summer HCB season in Clear Lake. From June to September of 2019 and 2020, the 10-day averaged wind speeds fluctuated between 2 and 5 ms^{-1}, while monthly average air temperatures ranged from 16.0 to 24.5 °C in 2019 and 17 to 25.6 °C in 2020 (Online Resource Fig. S.10). In 2021, on

the other hand, wind speeds declined from a peak in June throughout the summer and remained consistently below 3 ms^{-1}. Monthly air temperatures were warmer than in both previous years, with July (27.2 °C) and August (26.2 °C) being particularly hot. The combination of lower wind speeds and warmer air temperatures in 2021 resulted in the longest stratification event observed during the three summers, June 18–July 21. When a lake is stably stratified, cyanobacteria can use their buoyancy control ability to rise to the surface and outcompete other photosynthetic organisms for sunlight (Oliver et al. 2012). During this particularly long stratification event, cyanobacteria covered over 85% of the lake's surface area (Fig. 3). In contrast, during the previous two summers, stratification periods ranged from only 3 to 10 days when the HCB seasons were relatively mild. Furthermore, thermal stratification isolated the hypolimnion from oxygenated surface waters, leading to rapid oxygen depletion at depth and longer periods of time for anoxic P fluxes from lake sediments. As a result, both SRP and TP concentrations were higher in 2021 than in previous summers. Low spring discharge followed by warm stably stratified summers appear to influence interannual HCB variability in Clear Lake.

Comparative estimates of internal load

The discrepancy in L_{int} estimates (Table 3) highlights the fundamental differences and limitations of each method (Burnet and Wilhelm 2021; Nürnberg 2009a, b). L_{int_1} provides the most direct and intuitive quantification of internal P loading, as it is based on measured increases in water column nutrient concentrations during the dry season. However, this method aggregates all potential internal P sources (e.g., mineralization of organic P, mechanical resuspension, and redox-dependent sediment fluxes), obfuscating the relative contribution and timing of each mechanism. Furthermore, this method may underestimate the internal loading if sampling events are not frequent enough to capture peak nutrient concentrations in the water column. L_{int_1}, however, does provide an observation-based benchmark against which to compare theoretical estimates.

In contrast, L_{int_2} quantifies the theoretical gross internal load released from sediments, excluding other mechanical or biological release mechanisms. In the OA and the LA, 2019 L_{int_2} calculated with RR_{core} and RR_{TP} agreed closely with one another, corroborating our hypothesis that despite frequent vertical mixing events, redox-dependent diffusive flux from lake sediments is the primary mechanism of internal loading in these two arms of the lake. Compared with published release rates from other hypereutrophic reservoirs ($n = 21$, Carter and Dzialowski 2012; Nürnberg 1988), the UA sites have relatively low release rates, while the other sites were about average. However, $L_{int\_2\_TP}$ estimates for the

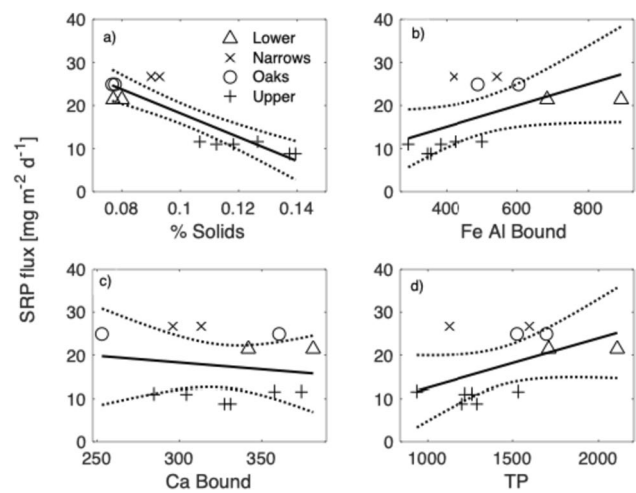**Fig. 10** Comparison of sediment composition with SRP release rates in lab incubation experiments. Sediment concentrations are units of μg g^{-1} and are average of the top 0–5 cm from duplicate oxic incubated cores, while SRP release rates shown are from anoxic cores. The solid line indicates least-squares linear regression with a 95% confidence interval (dotted line)

UA were 60% (2019)–110% (2021) larger than $L_{int\_2\_Core}$. Duplicate cores from all three UA sites had lower RR values than in the other arms, so this discrepancy is not likely the result of higher spatial heterogeneity than found in the other arms. Lower diffusive flux from UA sites may partially be explained by variation in sediment P composition (Fig. 10). UA cores contained the lowest concentrations of both TP and Fe/Al-bound P, the most labile P form, in the top 5 cm of profundal sediments. Previous research has shown that concentrations of Fe-bound P (Messer et al. 1984) and TP (Nürnberg 1988) in sediment are closely correlated with anoxic P release rates. Therefore, the lower observed RR values in UA cores likely reflect a smaller mobile P pool in UA sediments available for release. In addition, there was significant negative correlation between percent solids of the sediment (i.e., the total amount of solid material remaining after desiccating the sample) and SRP fluxes ($R^2 = 0.78$, $p < 0.001$). With a greater percentage of solids in sediments, there is less interstitial pore space where high rates of diffusion of P from solid to aqueous phase can occur. In 2020 and 2021, on the other hand, estimates from $L_{int\_2\_core}$ were significantly less than $L_{int\_2\_TP}$ in all arms, suggesting that seasonal variation in sediment P pools needs to be considered, especially in polymictic lakes, highlighting the limitations when modeling multi-year internal loads from an individual incubation experiment. While the magnitude of the internal loading varied by up to 40% depending on the method employed, both the gross and net estimates demonstrate that internal P loading during the summer/fall, not external loading, is the primary factor driving seasonal nutrient fluctuations in Clear Lake.

Monitoring the response of Clear Lake to management and restoration programs requires accurately capturing the spatial and temporal variation of water quality, hypoxia, and nutrient loadings across the lake. Examining the strengths and limitations of the various methods we employed to quantify basin-wide gross and net internal loads can be instructive for improving loading estimates in other polymictic systems. Due to labor and financial constraints, L_{int_1} is often the preferred method for determining loading rates in reservoirs (Burnet and Wilhelm 2021). However, this method assumes that measurements from monitoring sites are representative. In the UA, we observed within-basin variation in peak TP and SRP concentrations up to 23% and 24%, respectively. In contrast, net loading calculations for OA and LA were estimated from one monitoring site each, and thus there is uncertainty when assuming spatially homogenous concentrations across each sub-basin. Previous tracer studies have indicated that when stratified, baroclinic gradients and wind forcing can drive high dispersion rates and interbasin exchange of constituents throughout Clear Lake (Rueda et al. 2008). As a result, there can be significant intra- and inter-basin variability in nutrient concentrations. While individual point measurements may be sufficient for detecting long-term trends in eutrophication, distributed sampling strategies are necessary to accurately quantify internal loads in shallow lakes that are strongly influences by advective processes.

In addition, correctly determining the extent and duration of sediment anoxia can be challenging in shallow lakes with complex morphometry. In deep, stratified environments, the anoxic/hypoxic zone evolves in a predictable manner, forming first in the deep pelagic zone and growing vertically towards the shoreline until fall turnover ventilates the hypolimnion. When stably stratified, periodic vertical DO profiles are sufficient to determine the spatial extent of the actively releasing sediment area. However, in shallow polymictic systems, intermittent periods of stratification and mixing can deplete the hypolimnion of oxygen or rapidly reaerate it such that routine profile sampling may fail to accurately capture these changes. High-frequency in situ DO measurements, on the other hand, provided a more precise record of the timing and inter-basin variability of hypoxia. While AA_{mod} is frequently used to estimate the seasonal extent of sediment anoxia in polymictic systems, it does not indicate the timing of hypoxic events at time-scales relevant to ecosystem processes. By utilizing in situ measurements, we were able to precisely determine at an hourly time step when hypolimnetic DO concentrations would promote redox-dependent sediment P releases and when mixing events occurred that facilitated the transport of nutrient-enriched hypolimnetic waters to the photic zone for biotic uptake. Such high-frequency data can help to better quantify the physical and biogeochemical processes that influence interannual variability in cyanobacteria blooms in polymictic systems.

Unresolved internal loading mechanisms

The discrepancy between modeled and experimentally determined loading rates in the UA suggests that additional mechanisms are contributing to internal P loading in this arm. Despite containing the lowest sediment concentrations of TP and Fe/Al-bound P (Fig. 10), peak TP concentrations were consistently observed in the UA sites each summer. This may appear counterintuitive, as diffusive P fluxes are generally correlated with sediment P content (Nürnberg 1988). However, this trend is consistent with routine water quality and sediment sampling data collected by the LCWRD over the last 15 years (County of Lake Water Resources Department 2022), which measured lower sediment TP concentrations throughout the year and higher peak water column TP concentrations in the UA when compared with OA and LA sites. Increased loading in the UA can be partially explained by the longer periods of thermal stratification and a higher surface area-to-volume ratio. However, the discrepancy between experimental (RR_{core}) and modeled (RR_{TP}) sediment release rates in the UA indicate that additional mechanical (resuspension), chemical (pH), and biological (e.g., decomposition, translocation by cyanobacteria) processes are contributing to P cycling in this arm specifically.

In shallow lakes, physical processes such as wind stirring, wave action, boat wakes, benthivorous fish activity, and bioturbation by benthic infauna can disturb sediment, redistributing P-enriched water through the water column, enhancing P exchange (Steinman and Spears 2020). Wind-driven sediment resuspension has been identified as an important physical P-loading mechanism in many shallow, eutrophic systems, (Havens et al. 2007; Huang et al. 2016; Tammeorg et al. 2013), and experiments have shown that P fluxes from resuspended material can be 20–30 times greater than from undistributed sediments (Søndergaard et al. 1992). The dynamic ratio (i.e., inverse of the morphometric factor, *DR*) quantifies the susceptibility of a basin to wind-driven resuspension, with basins above a threshold of 0.8 generally being classified as highly susceptible (Havens et al. 2007). At Clear Lake, only the UA exceeds this threshold (Table 1), adding credibility to the hypothesis that sediment resuspension, during the summer and fall, may release TP in the shallow littoral regions. During the dry 2020 and 2021 years, the summertime water level declined by more than 1 m from 2019, significantly increasing the surface area susceptible to wind-driven resuspension (Laenen et al. 1996). Higher rates of sediment resuspension may in part have contributed to higher TP concentrations during a drought in the early 1990s.

Another potential mechanism is photosynthetically elevated pH driving higher release rates in littoral zones, as the pH of a waterbody influences the capacity of sediment to bind P. At high pH values, hydroxyl ions replace P on iron particle binding sites, leading to a decline in the capacity of oxidized surfaces to bind P (Jensen and Andersen 1992; Orihel et al. 2017). As photosynthesis results in elevated pH, high productivity events can increase P release (Koski-Vähälä and Hartikainen 2001). However, pH varied by less than 1 (7.7–8.7) between basins during the summer, indicating that this mechanism is unlikely to drive higher release rates in the UA specifically. Phosphorus translocation by migrating cyanobacteria, such as *Gloeotrichia*, can also contribute to internal loading in shallow lakes (Barberio and Welch 1992). However, given that *Gloeotrichia* was primarily observed in LA and OA (Fig. 6), this mechanism also does not explain the high P concentrations in the UA.

In addition, the decomposition of organic material can constitute a significant organic P input, as phosphorus is incorporated into numerous biomolecules (Orihel et al. 2017). Surface-catalyzed hydrolysis, photolysis, and mineralization by microbial activity can in turn mobilize and convert this solid organic P into an aqueous phase (Orihel et al. 2017; Reitzel et al. 2007). A biological survey of Clear Lake documented that the majority of rooted aquatic vegetation is found along the northern and western shallow regions of the UA (ReMetrix 2003), indicating that there is potential for higher rates of mineralization of aquatic vegetation in the UA relative to the deeper arms. However, few measurements of organic matter in Clear Lake sediments have been collected to date. Future research should focus on investigating the role that each of these factors play in contributing to P cycling between sediments and the water column in Clear Lake.

Conclusions

Net and gross internal P loads for Clear Lake were calculated for a 3-year period using two comparative methods to determine the relative contribution of external and internal loading to the system. Internal P loading accounted for 70–95% of the TP mass observed in Clear Lake annually with higher loading observed during drought years. The release of P during hypoxic periods shifted the system towards N limitation, favoring the proliferation of HCBs. N-fixing cyanobacteria, input additional N throughout the summer, facilitating the subsequent growth of non-N-fixing toxin-producing cyanobacteria, like *Microcystis*, in the fall. With climate change expected to promote longer and more intense periods of thermal stratification in temperate lakes, state and federal agencies should prioritize funding of in-lake strategies to mitigate HCBs in impaired water bodies. Engineering solutions such as hypolimnetic oxygenation, sediment dredging, and alum application are clearly needed in conjunction with watershed restoration projects to limit the availability of in-lake nutrients fueling these blooms in the short and long term.

Declarations

Conflict of interest The authors declare that they have no conflict of interest.

References

Abrantes N, Antunes SC, Pereira MJ, Gonçalves F (2006) Seasonal succession of cladocerans and phytoplankton and their interactions in a shallow eutrophic lake (Lake Vela, Portugal). Acta Oecologica 29(1):54–64. https://doi.org/10.1016/j.actao.2005.07.006

Aráoz R, Molgó J, Tandeau de Marsac N (2010) Neurotoxic cyanobacterial toxins. Toxicon 56(5):813–828. https://doi.org/10.1016/j.toxicon.2009.07.036

Barberio RP, Welch EB (1992) Contribution of benthic blue-green algal recruitment to lake populations and phosphorus translocation. Freshw Biol 27(2):249–260. https://doi.org/10.1111/j.1365-2427.1992.tb00537.x

Big Valley EPA (2021) 2021 clear lake cyanotoxin monitoring program

Bláha L, Babica P, Maršálek B, Luděk Bláha A (2009) Toxins produced in cyanobacterial water blooms-toxicity and risks. Interdisc Toxicol 2(2):36–41. https://doi.org/10.2478/v10102-009-0006-2

Boehme J, Schulhauser R, Bejankiwar R (2011) Atmospheric deposition of phosphorus to freshwater lakes

Burger DF, Hamilton DP, Pilditch CA (2008) Modelling the relative importance of internal and external nutrient loads on water column nutrient concentrations and phytoplankton biomass in a shallow polymictic lake. Ecol Model 211(3–4):411–423. https://doi.org/10.1016/j.ecolmodel.2007.09.028

Burnet SH, Wilhelm FM (2021) Estimates of internal loading of phosphorus in a western US reservoir using 3 methods. Lake Reserv Manag 37(3):261–274. https://doi.org/10.1080/10402381.2021.1923590

Carter LD, Dzialowski AR (2012) Predicting sediment phosphorus release rates using landuse and water-quality data. Freshw Sci 31(4):1214–1222. https://doi.org/10.1899/11-177.1

Chamberlin CE, Chaney R, Finney B, Hood M, Lehamn P, Mckee M, Willis R (1990) Abatement and control study: sulphur bank mine and clear lake

Chorus I, Falconer IR, Salas HJ, Bartram J (2000) Health risks caused by freshwater cyanobacteria in recreational waters. J Toxicol Environ Health B Crit Rev 3(4):323–347. https://doi.org/10.1080/109374000436364

Cortés A, Forrest AL, Sadro S, Stang AJ, Swann M, Framsted NT, Thirkill R, Sharp SL, Schladow SG (2021) Prediction of hypoxia in eutrophic polymictic lakes. Water Resour Res. https://doi.org/10.1029/2020WR028693

County of Lake Department of Public Works Water Resources Division (2010) Clear lake integrated watershed management plan

County of Lake Water Resources Department (2022) Clear lake limnological ambient water quality monitoring program (CLLAMP). https://ceden.waterboards.ca.gov/

Coveney MF, Lowe EF, Battoe LE, Marzolf ER, Conrow R (2005) Response of a eutrophic, shallow subtropical lake to reduced nutrient loading. Freshw Biol 50(10):1718–1730. https://doi.org/10.1111/j.1365-2427.2005.01435.x

De Palma-Dow A, McCullough IM, Brentrup JA (2022) Turning up the heat: long-term water quality responses to wildfires and climate change in a hypereutrophic lake. Ecosphere. https://doi.org/10.1002/ECS2.4271

Dillon PJ, Rigler FH (1974) The phosphorus-chlorophyll relationship in lakes. Limnol Oceanogr 19(5):767–773. https://doi.org/10.4319/lo.1974.19.5.0767

Ding S, Chen M, Gong M, Fan X, Qin B, Xu H, Gao SS, Jin Z, Tsang DCW, Zhang C (2018) Internal phosphorus loading from sediments causes seasonal nitrogen limitation for harmful algal blooms. Sci Total Environ 625:872–884. https://doi.org/10.1016/j.scitotenv.2017.12.348

Dolman AM, Mischke U, Wiedner C (2016) Lake-type-specific seasonal patterns of nutrient limitation in German lakes, with target nitrogen and phosphorus concentrations for good ecological status. Freshw Biol 61(4):444–456. https://doi.org/10.1111/fwb.12718

Domagalski JL, Morway E, Alvarez NL, Hutchins J, Rosen MR, Coats R (2021) Trends in nitrogen, phosphorus, and sediment concentrations and loads in streams draining to Lake Tahoe, California, Nevada, USA. Sci Total Environ. https://doi.org/10.1016/j.scitotenv.2020.141815

Eimers MC, Winter JG (2005) State of Lake Simcoe water quality 2000–2013. Newmarket, ON.

Einsele W (1936) Über die Beziehungen des Eisenkreislaufs zum Phosphatkreislauf im eutrophen. Archi Hydrobiol 29:664–686

Florea, K., B. Stewart, E. Webb, D. Caron, and J. Smith. 2022. Environmental drivers of cyanobacterial harmful algal blooms and cyanotoxins in clear lake: 2020–2021.

Guildford SJ, Hecky RE (2000) Total nitrogen, total phosphorus, and nutrient limitation in lakes and oceans: is there a common relationship? Limnol Oceanogr 45(6):1213–1223

Håkanson L (2004) Break-through in predictive modelling opens new possibilities for aquatic ecology and management—a review. Hydrobiologia 518(1–3):135–157. https://doi.org/10.1023/B:HYDR.0000025064.26497.53

Hanington P, Rose A, Johnstone R (2016) The potential of benthic iron and phosphorus fluxes to support the growth of a bloom forming toxic cyanobacterium *Lyngbya majuscula*, Moreton Bay, Australia. Mar Freshw Res 67(12):1918–1927. https://doi.org/10.1071/MF15219

Havens KE, Jin KR, Iricanin N, James RT (2007) Phosphorus dynamics at multiple time scales in the pelagic zone of a large shallow lake in Florida, USA. Hydrobiologia 581(1):25–42. https://doi.org/10.1007/s10750-006-0502-8

Holdren GC, Armstrong DE (1980) Factors affecting phosphorus release from intact lake sediment cores. Environ Sci Tech 14(1):79–87. https://doi.org/10.1021/es60161a014

Horne AJ, Goldman CR (1972) Nitrogen fixation in Clear Lake, California. I. Seasonal variation and the role of heterocysts. Limnol Oceanogr 17(5):678–692. https://doi.org/10.4319/lo.1972.17.5.0678

Horne AJ (1975) The ecology of clear Lake Phytoplankton

Huang L, Fang H, He G, Jiang H, Wang C (2016) Effects of internal loading on phosphorus distribution in the Taihu Lake driven by wind waves and lake currents. Environ Pollut 219:760–773. https://doi.org/10.1016/j.envpol.2016.07.049

Hupfer M, Lewandowski J (2008) Oxygen controls the phosphorus release from lake sediments—a long-lasting paradigm in limnology. Int Rev Hydrobiol 93(4–5):415–432. https://doi.org/10.1002/iroh.200711054

Iiames JS, Salls WB, Mehaffey MH, Nash MS, Christensen JR, Schaeffer BA (2021) Modeling anthropogenic and environmental influences on freshwater harmful algal bloom development detected by MERIS over the central United States. Water Resour Res. https://doi.org/10.1029/2020WR028946

Isles PDF, Giles CD, Gearhart TA, Xu Y, Druschel GK, Schroth AW (2015) Dynamic internal drivers of a historically severe cyanobacteria bloom in Lake Champlain revealed through comprehensive monitoring. J Great Lakes Res 41(3):818–829. https://doi.org/10.1016/j.jglr.2015.06.006

Jassby AD, Reuter JE, Axler RP, Goldman CR, Hackley SH (1994) Atmospheric deposition of nitrogen and phosphorus in the annual nutrient load of Lake Tahoe (California-Nevada). Water Resour Res 30(7):2207–2216. https://doi.org/10.1029/94WR00754

Jensen HS, Andersen FO (1992) Importance of temperature, nitrate, and pH for phosphate release from aerobic sediments of four shallow, eutrophic lakes. Limnol Oceanogr 37(3):577–589. https://doi.org/10.4319/lo.1992.37.3.0577

Kane DD, Conroy JD, Peter Richards R, Baker DB, Culver DA (2014) Re-eutrophication of Lake Erie: correlations between tributary nutrient loads and phytoplankton biomass. J Great Lakes Res 40(3):496–501. https://doi.org/10.1016/j.jglr.2014.04.004

Koski-Vähälä J, Hartikainen H (2001) Assessment of the risk of phosphorus loading due to resuspended sediment. J Environ Qual 30(3):960–966. https://doi.org/10.2134/jeq2001.303960x

Lake County Watershed Protection District (2009) Clear lake watershed TMDL monitoring program

Liikanen A, Murtoniemi T, Tanskanen H, Väisänen T, Martikainen PJ (2002) Effects of temperature and oxygen availability on greenhouse gas and nutrient dynamics in sediment of a eutrophic mid-boreal lake. Biogeochem 59:269–286

Lunetta RS, Schaeffer BA, Stumpf RP, Keith D, Jacobs SA, Murphy MS (2015) Evaluation of cyanobacteria cell count detection derived from MERIS imagery across the eastern USA. Remote

Sens Environ 157:24–34. https://doi.org/10.1016/j.rse.2014.06.008

Messer JJ, Ihnat JM, Wegner DL (1984) Phosphorus release from the sediments of Flaming Gorge Reservoir, Wyoming, USA. Verh Internat Verein Limnol 22(3):1457–1464. https://doi.org/10.1080/03680770.1983.11897518

Mills MM, Ridame C, Davey M, La Roche J, Geider RJ (2004) Iron and phosphorus co-limit nitrogen fixation in the eastern tropical North Atlantic. Nat 429(6989):292–294. https://doi.org/10.1038/nature02550

Mishra S, Stumpf RP, Schaeffer BA, Werdell PJ, Loftin KA, Meredith A (2019) Measurement of cyanobacterial bloom magnitude using satellite remote sensing. Sci Rep. https://doi.org/10.1038/s41598-019-54453-y

Molot LA, Young J, Dillon PJ, Hakanson L, Soliman C (2010) Intermin report on phosphorus and dissolved oxygen modelling of Lake Simcoe

Moore PA, Reddy KR Jr, Fisher MM (1998) Phosphorus Flux between Sediment and Overlying Water in Lake Okeechobee, Florida: spatial and temporal variations. J Environ Qual 27(6):1428–1439

Mortimer CH (1941) The exchange of dissolved substances between mud and water in lakes. J Ecol 29:280–329. https://doi.org/10.2307/2256395

Nürnberg GK (1988) Prediction of phosphorus release rates from total and reductant-soluble phosphorus in anoxic lake sediments. Can J Fish Aquat Sci 45(3):453–462. https://doi.org/10.1139/f88-054

Nürnberg GK (1996) Trophic state of clear and colored, soft- and hardwater lakes with special consideration of nutrients, anoxia, phytoplankton and fish. Lake Reserv Manag 12(4):432–447. https://doi.org/10.1080/07438149609354283

Nürnberg GK (2005) Quantification of internal phosphorus loading in polymictic lakes. Verh Internat Verein Limno 29(2):623–626. https://doi.org/10.1080/03680770.2005.11902753

Nürnberg GK (2009a) Assessing internal phosphorus load—problems to be solved. Lake Reserv Manag 25(4):419–432. https://doi.org/10.1080/00357520903458848

Nürnberg GK (2009b) Assessing internal phosphorus load—problems to be solved. Lake Reserv Manag 25(4):419–432. https://doi.org/10.1080/00357520903458848

Nürnberg GK, LaZerte BD (2016) More than 20 years of estimated internal phosphorus loading in polymictic, eutrophic Lake Winnipeg, Manitoba. J Great Lakes Res 42(1):18–27. https://doi.org/10.1016/j.jglr.2015.11.003

Nürnberg GK, Lazerte BD, Sun Loh P, Molot LA (2013a) Quantification of internal phosphorus load in large, partially polymictic and mesotrophic Lake Simcoe, Ontario. J Great Lakes Res 39:271–279

Nürnberg GK, Molot LA, O'Connor E, Jarjanazi H, Winter J, Young J (2013b) Evidence for internal phosphorus loading, hypoxia and effects on phytoplankton in partially polymictic Lake Simcoe, Ontario. J. Great Lakes Res 39(2):259–270. https://doi.org/10.1016/j.jglr.2013.03.016

Ogdahl ME, Steinman AD, Weinert ME (2014) Laboratory-determined phosphorus flux from lake sediments as a measure of internal phosphorus loading. J vis Exp 85:1–9. https://doi.org/10.3791/51617

Oliver R, Hamilton D, Brookes JD, George GG (2012) Physiology, blooms and prediction of planktonic cyanobacteria. In: Whitton BA (ed) Ecology of cyanobacteria II: their diversity in space and time. Springer, Berlin

Orihel DM, Schindler DW, Ballard NC, Graham MD, O'Connell DW, Wilson LR, Vinebrooke RD (2015) The 'nutrient pump:' Iron-poor sediments fuel low nitrogen-to-phosphorus ratios and cyanobacterial blooms in polymictic lakes. Limnol Oceanogr 60(3):856–871. https://doi.org/10.1002/lno.10076

Orihel DM, Baulch HM, Casson NJ, North RL, Parsons CT, Seckar DCM, Venkiteswaran JJ (2017) Internal phosphorus loading in Canadian fresh waters: a critical review and data analysis. Ca J Fish Aquat Sci 74(12):2005–2029

Paerl HW, Fulton RS, Moisander PH, Dyble J (2001) Harmful freshwater algal blooms, with an emphasis on cyanobacteria. Sci World J 1:76–113. https://doi.org/10.1100/tsw.2001.16

Peng H, Long F, Ding C (2005) Feature selection based on mutual information: criteria of max-dependency, max-relevance, and min-redundancy. IEEE Trans Pattern Anal Mach Intell 27(8):1226–1238

Redfield AC (1958) The biological control of chemical factors in the environment. Am Sci 46(3):205–221

Reitzel K, Ahlgren J, DeBrabandere H, Waldebäck M, Gogoll A, Tranvik L, Rydin E (2007) Degradation rates of organic phosphorus in lake sediment. Biogeochem 82(1):15–28. https://doi.org/10.1007/s10533-006-9049-z

ReMetrix (2003) Assessment of Clear Lake, CA For submersed aquatic vegetation, morphology, and sediment

Summary Report on Metals and Metalloids in Clear Lake Based on Historical Data (2022)

Richerson S, Why J, Suchanek TH (1994) The causes and control of algal blooms in clear lake, California

Rueda F, Schaldow G, Clark J (2008) Mechanisms of contaminant transport in a multi-basin lake. Ecol App Supp 18(8):72–88. https://doi.org/10.1890/06-1617.1

San Francisco Estuary Institute (2022) HAB satelite analysis tool. https://fhab.sfei.org

Schindler DW, Carpenter SR, Chapra SC, Hecky RE, Orihel DM (2016) Reducing phosphorus to curb lake eutrophication is a success. Environ. Sci. Tech. 50(17):8923–8929. https://doi.org/10.1021/acs.est.6b02204

Sharp SL, Forrest AL, Bouma-Gregson K, Jin Y, Cortés A, Schladow SG (2021) Quantifying scales of spatial variability of cyanobacteria in a large, eutrophic lake ssing multiplatform remote sensing tools. Front Environ Sci 9(April):1–19. https://doi.org/10.3389/fenvs.2021.612934

Sims JD (1988) Diatom biostratigraphy and the paleolimnology of Clear Lake, Lake County, California. In: Sims, JD (ed) GSA Special Papers, vol 214. Geological Society of America. https://doi.org/10.1130/SPE214

Smith VH (1983) Low nitrogen to phosphorus ratios favor dominance by blue-green algae in lake phytoplankton. Sci 221(4611):669–671

Smith VH (1985) Predictive models for the biomass of blue-green algae in lakes. J Clim 21(3):433–439. https://doi.org/10.1111/j.1752-1688.1985.tb00153.x

Smith VH, Schindler DW (2009) Eutrophication science: where do we go from here? Trends Ecol Evol. https://doi.org/10.1016/j.tree.2008.11.009

Smucker NJ, Beaulieu JJ, Nietch CT, Young JL (2021) Increasingly severe cyanobacterial blooms and deep water hypoxia coincide with warming water temperatures in reservoirs. Glob Change Biol 27(11):2507–2519. https://doi.org/10.1111/gcb.15618

Søndergaard M, Jensen JP, Jeppesen E (2001) Retention and internal loading of phosphorus in shallow, eutrophic lakes. Sci World 1:427–442. https://doi.org/10.1100/tsw.2001.72

Søndergaard M, Jensen JP, Jeppesen E (2003) Role of sediment and internal loading of phosphorus in shallow lakes. Hydrobiologia 506–509:135–145. https://doi.org/10.1023/B:HYDR.0000008611.12704.dd

Søndergaard M, Kristensen P, Jeppesen E (1992) Phosphorus release from resuspended sediment in the shallow and wind-exposed Lake Arreso, Denmark. Hydrobiologia

Song K, Burgin AJ (2017) Perpetual phosphorus cycling: eutrophication amplifies biological control on internal phosphorus loading in agricultural reservoirs. Ecosystems 20(8):1483–1493. https://doi.org/10.1007/s10021-017-0126-z

Spears BM, Carvalho L, Perkins R, Kirika A, Paterson DM (2012) Long-term variation and regulation of internal phosphorus loading in Loch Leven. Hydrobiologia 681:23–33. https://doi.org/10.1007/978-94-007-4333-5

Steinman AD, Spears BM (2020) Internal phosphorus loading in lakes : causes, case studies, and management. J Ross Publishing.

Stumpf RP, Tomlinson MC, Calkins JA, Kirkpatrick B, Fisher K, Nierenberg K, Currier R, Wynne TT (2009) Skill assessment for an operational algal bloom forecast system. J Marine Syst 76(1–2):151–161. https://doi.org/10.1016/j.jmarsys.2008.05.016

Suchanek TH, Richerson PJ, Nelson DC, Eagles-Smith CA, Anderson DW, Cech JJ, Zierenberg R, Schladow G, Mount JF, McHatton SC, Slotton DG, Webber LB, Swisher BJ, Bern AL, Sexton M (2002) Evaluating and managing a multiply stressed ecosystem at clear lake, California: a holistic ecosystem approach. Manag Healthy Ecosyst Case Stud:1233–1265

Svirčev ZB, Tokodi N, Drobac D, Codd GA (2014) Cyanobacteria in aquatic ecosystems in Serbia: effects on water quality, human health and biodiversity. Syst Biodivers 12(3):261–270. https://doi.org/10.1080/14772000.2014.921254

Tammeorg O, Niemistö J, Möls T, Laugaste R, Panksep K, Kangur K (2013) Wind-induced sediment resuspension as a potential factor sustaining eutrophication in large and shallow Lake Peipsi. Aquat Sci 75(4):559–570. https://doi.org/10.1007/s00027-013-0300-0

Tammeorg O, Nürnberg G, Horppila J, Haldna M, Niemistö J (2020) Redox-related release of phosphorus from sediments in large and shallow Lake Peipsi: evidence from sediment studies and long-term monitoring data. J Great Lakes Res 46(6):1595–1603. https://doi.org/10.1016/j.jglr.2020.08.023

Tetra Tech (2004) Total maximum daily load for nutrients in clear Lake, Lake County, California Technical Report

Tipping E, Benham S, Boyle JF, Crow P, Davies J, Fischer U, Guyatt H, Helliwell R, Jackson-Blake L, Lawlor AJ, Monteith DT, Rowe EC, Toberman H (2014) Atmospheric deposition of phosphorus to land and freshwater. Environ Sci Process Impacts 16(7):1608–1617. https://doi.org/10.1039/c3em00641g

van Duin EHS, Aalderink RH, Lijklema L (1995) Light adaptation of oscillatoria agardhii at different time scales. Water Sci Tech 32(4):35–48. https://doi.org/10.1016/0273-1223(95)00677-X

Wang X, Smith K, Hyndman R (2006) Characteristic-based clustering for time series data. Data Min Knowl Disc 13(3):335–364. https://doi.org/10.1007/s10618-005-0039-x

Wilson SG (2015) Soil genesis, mineralogy and phosphorus dynamics of the clear lake volcanic field. University of California, Davis

Winder M, Reuter J, Schladow G (2010) Clear Lake Historical Data Analysis.

Winter JG, Dillon PJ, Futter MN, Nicholls KH, Scheider WA, Scott LD (2002) Total phosphorus budgets and nitrogen loads : lake Simcoe, Ontario (1990 to 1998). J Great Lakes Res 28(3):301–314. https://doi.org/10.1016/S0380-1330(02)70586-8

Wu Z, Zou R, Jiang Q, Elser JJ, Zhao L, Ye R, Liu Y (2020) What maintains seasonal nitrogen limitation in hyper-eutrophic Lake Dianchi? Insights from stoichiometric three-dimensional numerical modeling. Aquat Sci. https://doi.org/10.1007/s00027-020-00744-w

Wurtsbaugh WA, Horne AJ (1983) Iron in eutrophic Clear Lake, California: its importance for algal nitrogen fixation and growth. Can J Fish Aquat Sci 40(9):1419–1429. https://doi.org/10.1139/f83-164. (**NRC Research Press**)

Xu H, Paerl HW, Qin B, Zhu G, Hall NS, Wu Y (2015) Determining critical nutrient thresholds needed to control harmful cyanobacterial blooms in eutrophic Lake Taihu, China. Environ Sci Technol 49(2):1051–1059. https://doi.org/10.1021/es503744q

Publisher's Note Springer Nature remains neutral with regard to jurisdictional claims in published maps and institutional affiliations.